



Master Thesis

Ice Basement Mapping of Eisriesenwelt Cave with Ground Penetrating Radar

submitted by Ao Kaidong

born on 01.08.1993 in Hulunbuir, China

submitted for the academic degree of
Master of Science (M.Sc.)

Date of Submission 16.01.2018

Supervisors Prof. Dr. Manfred F.Buchroithner
Institute for Cartography, TU Dresden

Dr. –Ing. Holger Kumke
Chair of Cartography, TU München

Statement of Authorship

Herewith I declare that I am the sole author of the thesis named

„Ice Basement Mapping of Eisriesenwelt Cave with Ground Penetrating Radar“

which has been submitted to the study commission of geosciences today.

I have fully referenced the ideas and work of others, whether published or unpublished. Literal or analogous citations are clearly marked as such.

Dresden, 16.01.2018

Signature

St. Giday 郭 志 东

Acknowledgement

Firstly, I would give my sincere gratitude to the supervisor of this thesis, Prof. Dr. Manfred F. Buchroithner, thank you for sharing this excellent research topic with me and being always helpful. Furthermore, your enthusiasm for the cave and mountain researching did motivate me through the whole thesis work. And also, I would thank Mr. Benjamin Schröter for your guidance on my thesis, plus, the days we spend in Austria for this research was definitely a highlight during the whole master's programme, thank you!

Secondly, thank you Dr. Christoph Mayer for your kindly help on the instruments and the software. That was really super helpful! And Mr. Wilson Lampenwarti, thank you for your professional help and the company in the cave last spring, I hope I can see you soon again back in the wonderful Eisriesenwelt!

Moreover, to my friends and colleges in TU Munich, TU Wien and TU Dresden, I did enjoy and appreciate your help and company. That truly made my two and a half year of study so fun and cheerful. I will never forget the time we have spent together. Thank you all!

Especially, to my faithful friends Keni Han and Alika Jensen, your friendship and enthusiasm really mean a lot to me, thank you!

Last but not the least, Dad, Mom, school is over, thank you for everything you have done for me in these years.

Content

Statement of Authorship	2
Acknowledgement	3
Content	1
Figures.....	3
Tables	5
1 INTRODUCTION	6
1.1 Geographic Environment Of The Eisriesenwelt Cave	7
1.2 Surveying Methods of Ground Penetrating Radar.....	9
1.2.1 <i>Introduction of Ground penetrating radar</i>	9
1.2.2 <i>Surveying Methods</i>	10
1.3 Structure of the Thesis.....	11
1.4 Research Aims and Objects.....	12
1.4.1 <i>Aims</i>	12
1.4.2 <i>Objectives</i>	12
2 STUDY AREA AND DATA PREPARATION	12
2.1 Study Area.....	12
2.1.1 <i>The discovery and early explorations of the Eisriesenwelt cave</i>	12
2.1.2 <i>The classification of ice caves</i>	14
2.1.3 <i>Laser scanning and previous ice thickness measurements in ERW</i>	16
2.1.4 <i>The digitalization of study area in ERW</i>	17
2.2 BASIC PRINCIPLES OF GPR DATA.....	20
2.2.1 <i>GPR systems</i>	20
2.2.2 <i>GPR datasets</i>	23
2.3 GPR Data Pre-Processing	23
2.3.1 <i>Dewow Filtering</i>	24
2.3.2 <i>Time-zero correction</i>	25
2.3.3 <i>Gain functions</i>	26
2.3.4 <i>Trace editing</i>	30
2.4 Time-Depth Conversion of GPR Data.....	30
2.4.1 <i>Propagation velocity analysis</i>	31

2.4.2	<i>Data Migration</i>	32
2.4.3	<i>Layer analysis</i>	34
2.5	Elevation Extraction From Laser Scanned Dataset	35
3	METHODOLOGY	35
3.1	Electromagnetic Features of Subject and Radar Wave.....	37
3.2	Accuracy Assessment.....	39
3.3	Feature Points Extraction.....	42
3.4	Methodology of Depth Interpolation	44
3.5	Methodology of Map producing.....	45
4	RESULTS.....	47
5	CONCLUSION AND OUTLOOK	53
5.1	Conclusion.....	54
5.2	Outlook	55
	References	56

Figures

<i>Figure 1. Location of the Eisriesenwelt cave</i>	<i>7</i>
<i>Figure 2, Chimney effect of ERW cave (Eisriesen GmbH, 2016)</i>	<i>8</i>
<i>Figure 3. GPR scanning method (ScanTech Geoscience, 2017).....</i>	<i>9</i>
<i>Figure 4. Standardized GPR data process procedures</i>	<i>11</i>
<i>Figure 5. Ice Steps to Von Mörk Dom by Kaltenegger (J.W.Puttrell, 1932).....</i>	<i>13</i>
<i>Figure 6. Classification of ice caves (Luetscher and Jeannin, 2004).....</i>	<i>16</i>
<i>Figure 7. Survey lines marked on the map, positions of walking paths have been corrected</i>	<i>17</i>
<i>Figure 8. Rectified laser scanned data with digitalized walking paths</i>	<i>18</i>
<i>Figure 9. Screenshot of the virtual flyover</i>	<i>19</i>
<i>Figure 10. Digitalized study area with rectified laser scanned data</i>	<i>19</i>
<i>Figure 11. GPR data acquisition (A. Neal, 2004)</i>	<i>20</i>
<i>Figure 12. Display of Amplitude Difference of Raw GPR data on Reflexw Software</i>	<i>21</i>
<i>Figure 13. Installation of the RIS MF Hi-Mod GPR system</i>	<i>22</i>
<i>Figure 14. The wow effect on GPR signal (Harry M. Jol, 2009)</i>	<i>24</i>
<i>Figure 15. GPR signal after dewow filtering (Harry M. Jol, 2009).....</i>	<i>24</i>
<i>Figure 16. Example of time-zero correction in 0421AA GPR data section</i>	<i>25</i>
<i>Figure 17. Example of user-defined gain function applied on dataset 0421AE</i>	<i>27</i>
<i>Figure 18. Example of setting a user-defined deep feature enhancement gain function</i>	<i>27</i>
<i>Figure 19. Example of deconvolution filter applied on 200MHz GPR data (0421AE)</i>	<i>30</i>
<i>Figure 20, signal position correcting by diffraction hyperbola and corrected trace dips</i>	<i>33</i>
<i>Figure 21. The comparison between unmigrated data and migrated data.....</i>	<i>34</i>
<i>Figure 22. Estimation of ice-bedrock boundary layer</i>	<i>34</i>
<i>Figure 23. Methodology to ice basement mapping with GPR survey data.....</i>	<i>36</i>
<i>Figure 24. Quantificational model of electromagnetic wave between two materials (A. Neal, 2009)</i>	<i>39</i>
<i>Figure 25. Two resolutions of GPR system</i>	<i>40</i>
<i>Figure 26. The theoretical model of the Fresnel zone</i>	<i>41</i>
<i>Figure 27. Example of subsurface manual picking.....</i>	<i>43</i>
<i>Figure 28.Example of feature points picking.....</i>	<i>43</i>
<i>Figure 29, Ice basement map of Eisriesenwelt.....</i>	<i>47</i>
<i>Figure 30. Thematic map of ice thickness (Part I)</i>	<i>48</i>
<i>Figure 31. Thematic map of ice thickness (Part II)</i>	<i>49</i>

<i>Figure 32. Thematic map of ice thickness (Part III)</i>	<i>50</i>
<i>Figure 33. Thematic map of ice thickness (Part IV)</i>	<i>51</i>
<i>Figure 34. Thematic map of ice thickness (Part V)</i>	<i>52</i>
<i>Figure 35. Ice thickness distribution map of Eisriesenwelt</i>	<i>53</i>

Tables

<i>Table 1. Perennial ice occurrences in caves (Ford & Williams, 1989; Hill & Forti, 1997; Yonge, 2003)</i>	<i>15</i>
<i>Table 2, typical electrical properties of common subsurface materials (Hubbard and Glasser, 2005)</i>	<i>32</i>
<i>Table 3. Map symbols</i>	<i>46</i>

1 INTRODUCTION

“Ice caves” are rock-hosted caves containing perennial ice or snow, or both. The definition is proposed in accordance with the First International Workshop on Ice Caves (Căpuș, Romania, 2004). As an indicator of contemporary climate changes and potential paleoclimate archives, the presence, structure, and thickness of the cave ice which persists in ice caves have attracted significant attention since the beginning of the 20th century and are also subject to relatively recent investigation (Luetscher, 2005). This study focuses on presenting an overall view of the cave ice basement with the ice thickness of the ice cave Eisriesenwelt, which is known as the largest ice cave of the world, located in a southern Austrian Alpine mountain.

The survey of cave ice for this study is conducted on the behalf of the Institute for Cartography of Dresden University of Technology and the executive board of the Eisriesenwelt GmbH, Werfen, Austria. With Ground-penetrating Radar (GPR) type RIS MF Hi-Mod from IDS, provides dual-frequency antennas of 200MHz and 600MHz. The raw profile datasets, which were collected during the time period of the 20th to 24th April, 2017, consist of 115 vertical profiles of the ice body from various cave chambers.

The fundamental geophysical methodology of this study is based on the fact that the cave ice in Eisriesenwelt cave has existed for a relatively long time period up to approximately 1000 years. It can be thus classified as a permafrost phenomenon (H. Hausmann, 2010). Therefore, the physical and electromagnetic (EM) properties of permafrost earth materials can be applied to the ice body in this study. For the raw GPR dataset processing (time-depth migration), the physical properties and internal structures of the propagation medium are associated with the pattern of the radar pulse reflection.

Data is supported by a set of highly detailed three-dimensional Eisriesenwelt cave models based on laser scanning data obtained in previous cave scanning missions in 2010 and 2013. It was executed by the Institute for Cartography of Dresden University of Technology and thematic maps of ice basement display the ice basement details by giving a comprehensive overview of the cave ice thickness will be completed in this study.

Historical ice volume information has been collected by a comprehensive literature survey from 19 perennial ice caves of the Northern Hemisphere’s mid-latitudes. Records are detailed in the Appendix. The first ice cave records that offer potential volume references date back as early as 1907 in Europe, 1924 in North America, and 1927 in Asia. Seldom of the available

multi-decadal cave ice have volume histories showed a steady decreasing trend. Historical ice volume information summarized for 19 perennial ice caves on three continents of the Northern Hemisphere documented ca. 23,000m³ of cave ice loss until 2010. Improved research on the underground permafrost environment, as well as the underground ice bodies, which have been documented to suffer a significant mass loss worldwide, is a crucial topic with the global research heat on climate changes and the stabilities.

Moreover, determining interpolation parameters for interpolating the bedrock topography based on irregularly distributed GPR survey grids to approach a reasonable accuracy is found to be challenging. Due to the lack of the investigation of the electromagnetic wave speed in the ice body on this antennae, the wave speed parameters are based on the previous studies on this ice body. With the LiDAR scanning data support from previous missions in 2012 and 2013, a detailed ice surface can be digitalized, but known as a dynamic body, the ice coverage may have changed slightly since 2013.

1.1 Geographic Environment of The Eisriesenwelt Cave

Located in the Calcareous Austrian Alps, Southern Austria (Figure 1, the location of ERW cave is shown with a red star), Eisriesenwelt cave, also known as the World of Ice Giants, holds its importance as the largest ice cave in the area of the highest density of ice caves, also being the largest ice cave of the world. Eisriesenwelt cave (hereafter abbreviated as ERW) is a karst cave system with a total length of more than 40 kilometers, the major large entrance at the elevation of 1642m a.s.l. The ice-covered part with an ice thickness reaching meters level is ca. 800 meters, comprising a surface area of ca. 10000m² (Klappacher and Haseke Knapczyk, 1985).



Figure 1. Location of the Eisriesenwelt cave

There are numerous ice caves have been observed and thoroughly described around the world (Hill and Forti, 1997). Hill & Forti (1997) and Youge (2003) listed most of the cave ice patterns and referred to the major studies dedicated to them. According to which, the existence of cave ice mainly results from recrystallization of snow, freezing of infiltration water, including ponded ice, drip or flowstones or deposition of hoar frost (M Luetscher, PY Jeannin, 2004). For the ERW, the occurrence of the cave ice results mainly from the water infiltrating through the porous rock; due to the sub-zero temperature inside the cave, ice formation begins.

Since cave ice can be found either as permafrost or temperate regions, only a few caves can endure the existence of cave ice as permafrost; despite seasonal variations, the ERW cave is known as a dynamic ice cave with permafrost environment. In these permafrost regions, first, the annual mean temperatures are below zero, leading to the freezing of water and second, there exists a chimney effect, which is forced ventilation which caused by the initiation of cool air circulation in winter with multiple entrances at different elevations. Winter ventilation of the underground system is given by the density difference of the relatively warmer cave air and the cold outer air (B. May et al, 2011). In summer, the ventilation direction is reversed. The chimney effect (*figure 2*) is the predominant principle of the causing of a dynamic ice cave.

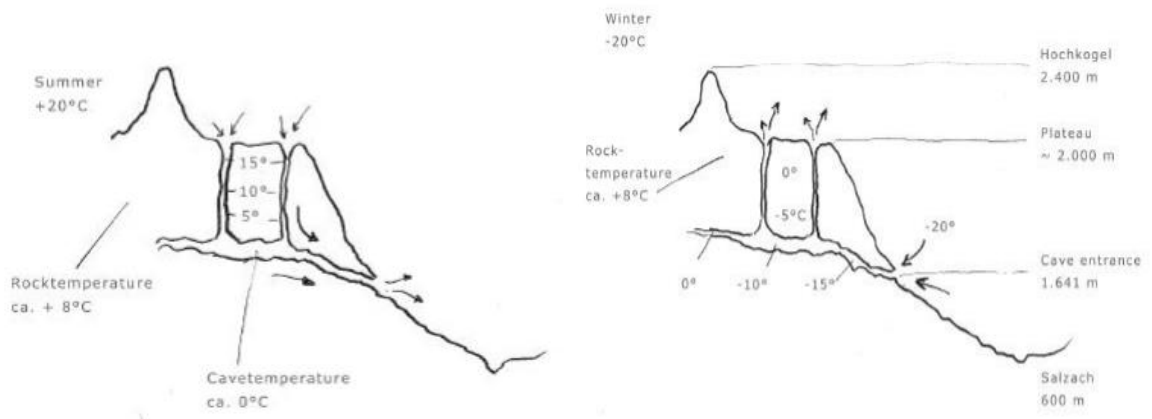


Figure 2, Chimney effect of ERW cave (Eisriesen GmbH, 2016)

1.2 Surveying Methods of Ground Penetrating Radar

1.2.1 Introduction of Ground penetrating radar

Ground penetrating radar (GPR) as a geophysical method of surveying is now well-accepted and widely applied. The method uses radio wave pulses to probe depth of tens of meters down through the ground, which records any low loss dielectric material. The non-destructive method transmits the electromagnetic radiation in the microwave band via antennas and detects the reflected signals from subsurface structures.

Ground penetrating radars have evolved their own natural set of terminology, common understandings, and practical application procedures. The first attempts obtained results on detecting subsurface structures were on the 1950s (El Said, 1956; Waite and Schmidt, 1961). Waite's demonstration of ice sheet sounding with aircraft radar altimeters lead to radio-echo sounding in many locations around the world. From this start, there was a gradual transition of the concepts to sounding soil and rock, which began in the 1960s and has continued ever since.

The transmitting depth of the electromagnetic wave pulses of a GPR is limited by the electrical conductivity of the ground, the center frequency of the transmitter, and the radiated power. As conductivity increases, the penetration depth decreases. With a higher conductivity, the EM energy is easier to dissipate into heat, resulting in a quick loss of signal strength in depth. Frequency has an impact on the resolution; a higher detection frequency gives a better resolution, also on penetrating depth, and the frequency of the antennae gives a distinctive variance. The two-way travel time of the recorded radiogram will be marked as the

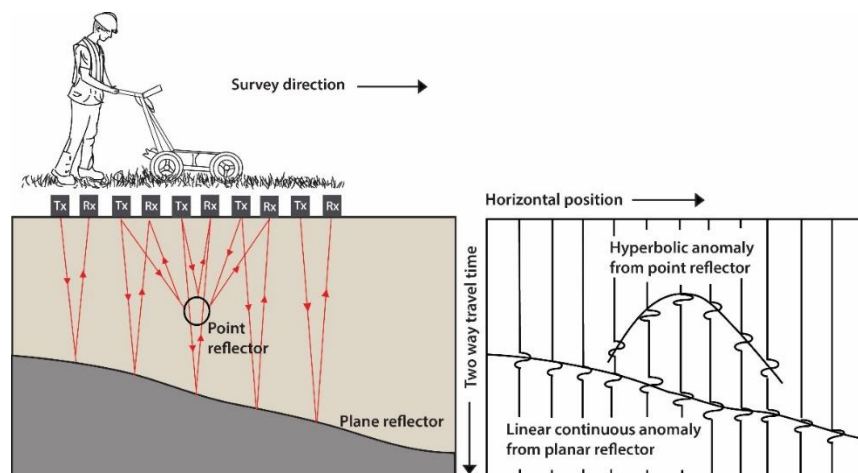


Figure 3. GPR scanning method (ScanTech Geoscience, 2017)

time unit in surveying, and the travel time will be converted to depth by relating it to on-site measurements or assumptions about the transmitting velocity of radar waves in the subsurface medium under investigation. In this study, the measurements were conducted on the ice surface, which is an ideal transmitting medium for GPR

1.2.2 *Surveying Methods*

Ground penetration radar has been used extensively in permafrost terrain, including studies of variations in active-layer thickness (Pilon et al., 1985; Doolittle et al., 1990, 1992; Moorman et al., 2003; Wu et al., 2005) and the relative dielectric permittivity of frozen sediments (Arcone and Delaney, 1989). Moreover, GPR has also been used to identify and map areas of massive ground ice (Kovacs and Morey, 1985; Dallimore and Davis, 1987). There are proven possibilities for GPR surveying of ice basements in ERW cave.

In this study, we used the RIS MF Hi-Mod instrument with a shielded dual-frequency antennae ranging from 200 to 600 MHz. All the data were obtained from the 200MHz frequency antennae, for a deep estimated depth of the ice surface. The trace sampling rate is 32 traces per second. The lateral trace space can be known with the overall trace quantities and the survey line length. On average it is about 0.032m.

Being known as a dynamic ice cave with a complicated inner structure and a vast difference of elevation, the ERW cave gives little chance to set an evenly distributed scanning network over all of the ice surface, but in the ice accumulating area like the Eispalast, a rather horizontal ice surface can be found. On this relatively horizontal surface, a scanning network was built with intervals between single scans smaller than 2m.

The raw data also needs to be processed and interpreted correctly, which usually includes automatic gain control (15ns length), 2D filtering, data migration, depth converting and data displaying. In this study, the electromagnetic waves transmitting velocity analysis are conducted based on the previous studies of the magnetic wave speed on permafrost medium and previous studies on the ice body of ERW cave. The standard data processing procedures see below (Figure 4).

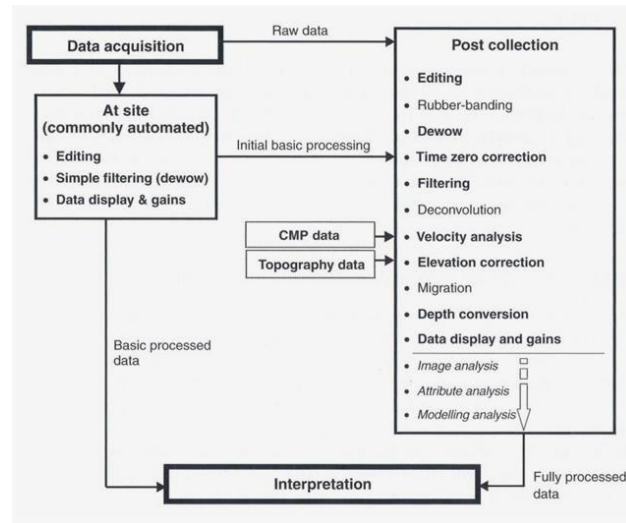


Figure 4. Standardized GPR data process procedures

1.3 Structure of the Thesis

This master's thesis is dedicated to mapping the ice basement of the Eisriesenwelt cave with the help of ground penetration radars. All the work addressed in this study is structured in five chapters, as shown below:

Chapter 1. INTRODUCTION

Chapter 2. DATA AND STUDY AREA

Chapter 3. METHODOLOGY

Chapter 4. RESULTS

Chapter 5. CONCLUSION AND OUTLOOK

In the first chapter, a brief introduction of this study is given and the potential problems are stated. Moreover, with the study motivation, the introduction of the study environment, and instruments, the research aims and objectives to be addressed are clarified. The second chapter will be focusing on the basic data sources and acquisition, and data pre-process procedures. The methods of study area (cave ice coverage) digitalization, the migration of pre-processed data, and time-depth conversion will also be included. The third chapter goes through the detailed GPR surveying methods which were used during the fieldwork,

data accuracy estimation, and migrated data interpolation method. The choice of interpolation methods for ice thickness sampling points will also be discussed in this chapter. In chapter four, the results will include a series of ice basement thematic maps. Conclusions and discussion of the study will be provided in the last chapter.

1.4 Research Aims and Objects

1.4.1 Aims

To evaluate, map the overall thickness distribution of the ice coverage of Eisrie-senwelt cave

1.4.2 Objectives

Collect the raw data of ice thickness

Collect the historical survey data of ERW cave

Determine the study area from the digitalized ice coverage

Pre-process the raw data, study the structure and features of GPR survey data

Post-process the GPR data, extracting depth sampling points

Compare the sampling methods, re-sampling depth points

Interpolate depth points

Produce thematic maps

2 STUDY AREA AND DATA PREPARATION

2.1 Study Area

2.1.1 *The discovery and early explorations of the Eisriesenwelt cave*

The Eisriesenwelt cave has not appeared on any official record before the October of 1879, due to its unavailability, both visual and physical.

By Anton von Posselt-Czorich (1854 - 1911), an Alpinist and a natural scientist, the Eisriesenwelt cave had the first recorded entrance, followed the local hunter called Eckschlager. In his



Figure 5. Ice Steps to Von Mörk Dom by Kaltenegger (J.W. Puttrel, 1932)

first exploring log, an ice cone with a diameter of about six meters and a height of seven meters was described, which was later on named "Posseltturm". With the help of crampons, the explorer pushed forward into the unknown cave around 200 meters, reached a vast ice wall.

On the 4th November 1879, Anton von Posselt-Czorich presented his discovery of this cave at the monthly meeting of the section Salzburg and published a report about this cave on the booklet of the German and Austrian Alpinist Association 1880.

The ERW cave has been kept uninvestigated for the next 33 years until Alexander von Mörk (1887 - 1914) noticed the report about this cave in 1911. On the 22nd November

1912, Alexander von Mörk and his team pushed further, successfully crossed over the vast ice wall. However, due to lack of equipment, they stuck at an ice wall about ten meters high. The next attempt of exploring was on 2nd August 1913, Alexander von Mörk along with Dr. Erwin von Angermayer and Herrmann Rihl pushed over the ice wall by building stairs on the ice (figure 4) which stopped them in 1912. They later on, discovered the so-called "Hymirhalle", which presents the largest growth of ice at the whole Eisriesenwelt cave. Changed with time, the most famous ice figure they discovered is commonly known as "Ice bear" due to its vastness. The cavers were stopped again by an underground lake called "Strumsee", where a stiff breeze blew. Later in the same month, a team consisting of Alexander von Mörk, Dr. Erwin von Angermayer, Herrmann Rihl, and Dr. Rudolf Freiherr von Saar, Dipl.-Ing. Walther Freiherr von Czoernig-Czernhausen, Rudolf Hardil, Dr. Hermann Klein, Grete Fahrner (Friedrich, 2009) entered the ice cave again. The first four dived through the lake with self-made diving suits.

The exploring team entered a vast hall with a height about 40 meters, which was later named “Alexander von Mörk Dom” to honor this early explorer.

Both Alexander von Mörk and Hermann Rihl have lost their lives in the World War I.

On the 28th September the Brothers Robert and Friedrich Oedl, Walter Czoernig-Czernhausen and Hermann Gruber discovered the colossal hall later called “Eispalast”, means ice palace. Behind the Eispalast there is a massive cave system without ice coverage. On 26th September 1920, the Eisriesenwelt cave opened for tourists.

2.1.2 *The classification of ice caves*

Traditionally, the ice caves were classified into two basic types: static and dynamic (THURY, 1861), based on cave air dynamics. The dynamical type is a crucial factor to describe the mass-energy ex-change in ice cave environments.

For static ice caves, according to THURY (1861), the signature-like downward sloping with a closed end conduits constrain the air circulation in summer seasons. Only when the condition that the air temperature outside of the cave is lower than the air temperature inside of the cave occurs, the air circulation happens. Such insignificant energy exchange results in a “cold air trap” in summer to keep the cave ice inside the cave.

For dynamic caves, the chimney effect plays a crucial role in keeping cool environments in dynamic ice caves. Due to the existence of multiple entrances located on different elevations, the air pressure and the air density difference at various entrance drives a single-direction air circulation. The air temperature inside the cave is nearly constant (Wigley and Brown, 1976; Choppy, 1984; Lesioned, 2002) while the external temperature varies seasonally. Therefore the chimney effect triggers chimney winds in reverse directions due to the temperature variations. In winter seasons, the cold air blows from the lower entrance to the higher ones enable infiltration water to freeze.

However, this classification theory does not provide the origin of cave ice. The following table (Table 1) gives perennial ice occurrences in caves (Ford and Williams, 1989; Hill and Forti, 1997; Yonge, 2003).

Adapted those two classification theories, Luetscher and Jeannin (2004) proposed a new nomenclature was distinguishing between congelation ice patterns and accumulated ice patterns, also air dynamic considerations. In *figure 6*, a synthesis of classification based on cave air dynamics criteria and classification based on ice formation processes is suggested.

Underline this classification method; the Eisriesenwelt cave is a typical dynamic cave with congelation ice due to the substantial chimney effect. In winter seasons, the internal air temperature is lower than external air temperature, so as air density, which causes cold air blows into the cave through the lower entrance meanwhile warm air blows out from the upper entrance. In summer, even though the warm air is observed to be sucked into the cave, but the cold air trap phenomenon is still non-negligible. The year-round constant cool air temperature environment inside the ERW cave triggered the freezing of infiltrating melting water result in the existence of a massive amount of stable cave ice.

Ice type	Description	Formation	Literature
Firn (recrystallized snow)	Opaque to bluish, layered	Accumulation of snow in cave traps which densifies and recrystallizes with infiltration component	e.g. MAIRE (1990); BINI & PELLEGRINI (1998)
Intrusive	Massive ice subliming on the caveward face or with hoarfrost formation	Glacier ice intruded into cave passages at the glacier/rock contact	e.g. FORD <i>et al.</i> (1976)
Drip or flowstone (congelation ice)	Stalactites, stalagmites, flowstone. Polycrystalline, clear to opaque	Freezing of infiltration water	e.g. RACOVITĂ (1994); PULINOWA & PULINA (1972); KYRLE (1923); VIEHMANN & RACOVITĂ (1968)
Ponded ice (congelation ice)	Clear or coarse polycrystalline ice. Occasionally with bubbles	Static water that freezes from the top downward. Can incorporate infiltration water and falling hoar ice	e.g. MARSHALL & BROWN (1974)
Hoar frost	Needles, rosettes and hexagonal plate crystals up to 0.5 m. Small, tapering prismatic crystals	Humid air condensing onto cave walls below 0°C	e.g. LAURIOL & CLARK (1993); WALDNER (1933); HALLIDAY (1966)
Ice in clastic sediments	Intra-particle aggregations as irregular masses, lenses, needles or soil-like extrusions	Freezing of moist sediments	e.g. PULINOWA & PULINA (1972); SCHROEDER (1977)
Extrusive	Curving fibrous crystals, similar to gypsum flowers up to 20 cm long	Supercooled water forced through microfissures in rock below 0°C which freezes as it emerges from the cave walls	e.g. FORD & WILLIAMS (1989)

Table 1. Perennial ice occurrences in caves (Ford & Williams, 1989; Hill & Forti, 1997; Yonge, 2003)

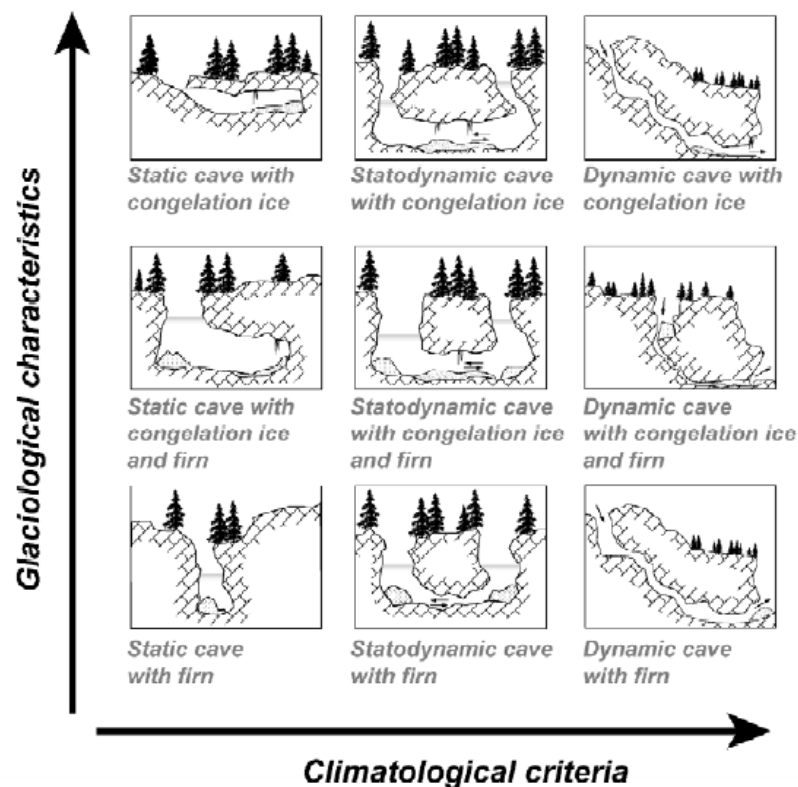


Figure 6. Classification of ice caves (Luetscher and Jeannin, 2004)

2.1.3 Laser scanning and previous ice thickness measurements in ERW

Starting in April 2010, Petters (2012) executed a three-dimensional survey and visualization project of the ice-filled part of the Eisriesenwelt. A considerable amount of laser scanned data has been collected as point clouds. Also, a workflow on data processing from separating the raw data, mesh generation to creating an autostereoscopic display was completed. This research also provided an accurate estimation of the ice surface area, which was determined to be 24,345 m².

In 2013, Beckert (2013) re-scanned the ice-filled part, with the data, a three-dimensional virtual model of the Eisriesenwelt was made. These two researchers provided significant support for the work of this thesis.

On the 16th October 2006, Behm and Hausmann (2007) measured the ice thickness with ground penetration radar. In part "Eispalast", Behm and Hausmann captured nine scanned profiles of the ice, with the help of steam drills. In their results, the 70-meter-high, 25-meter-wide chamber has a maximum ice thickness of 7.5 meters. However, a detailed ice thickness interpolation has not been presented.

2.1.4 The digitalization of study area in ERW

The Eisriesenwelt, world's most prominent ice cave has a total length more than 42km, an ice coverage range from 10,000m² (Eisriesenwelt Gesellschaft m.b.H., 2002) to 30,000m² (Friedrich, 2009). Therefore creating an accurate delineation of the ice coverage has essential importance in this research.

For delineating the cave ice coverage, for creating a relatively big scale cave map, manual delineation is regarded as the digitalization method with the most accurate comparing to automated digitalization methods (Tiwari, et al., 2016). The data support for ice coverage digitalization is multi-sourced. Includes a detailed cave map on the scale 1:1250, laser scanned data collected by Beckert (2013), field records from the field work and flyover footage made by Petters (2012) based on the laser scanned data.

During the field work for data acquisition, the surveying network was marked on an enlarged cave map made by Mag. Albert Morocutti, Dr. Dipl. Ing. R. Oedl, Dipl. Ing. W. Czoernig and G. Abel (*Figure 7*). This map covered the whole surveyed cave system with satisfactory accuracy, both ice-covered parts, and non-ice-covered parts. However, the map was finished in the 1970s, and the cave ice in the ERW cave can be regarded as a dynamic ice body, the details on this map may have changed. Moreover, the actual positions of walking paths for tourists on this map have been changed.

The laser scanned data of the ERW cave has been converted into a series of two-dimension images during the previous mission in 2013, from which, an accurate rectified image of the

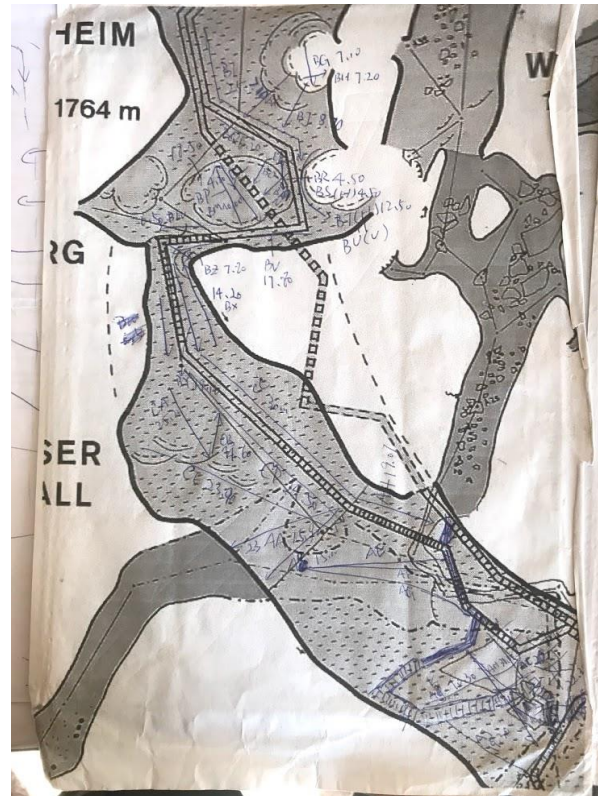


Figure 7. Survey lines marked on the map, positions of walking paths have been corrected

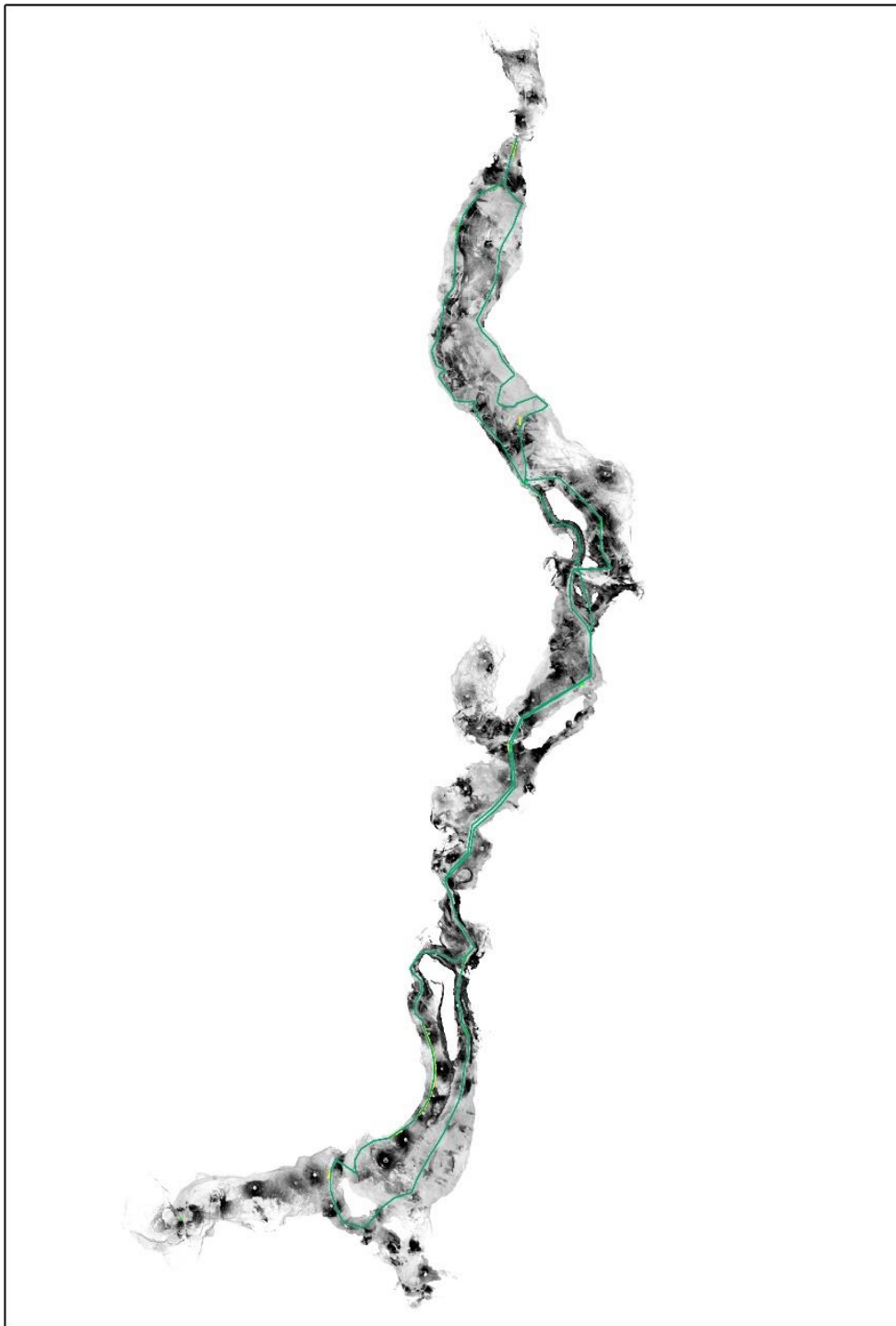


Figure 8. Rectified laser scanned data with digitalized walking paths

whole study area of the ice cave was made (Figure 8). From which the walking paths can be easily recognized, also some parts of the ice coverage.

With the virtual flyover footage (*Figure 9*), some unclear details of the ice coverage on both maps and images can be confirmed; it provided a solid assist on the digitalization work. In the following screenshot, the ice coverage is showed with a darker colour.



Figure 9. Screenshot of the virtual flyover

With the data support from the previous researchers, combined with the distribution of the GPR survey network, a study area of the ice surface (marked in blue) can be determined as figure 10 in this study.

In this study, only the profiles of a limited amount of vertical ice walls were taken into account. All the characteristic features in the profiles were included and examined.

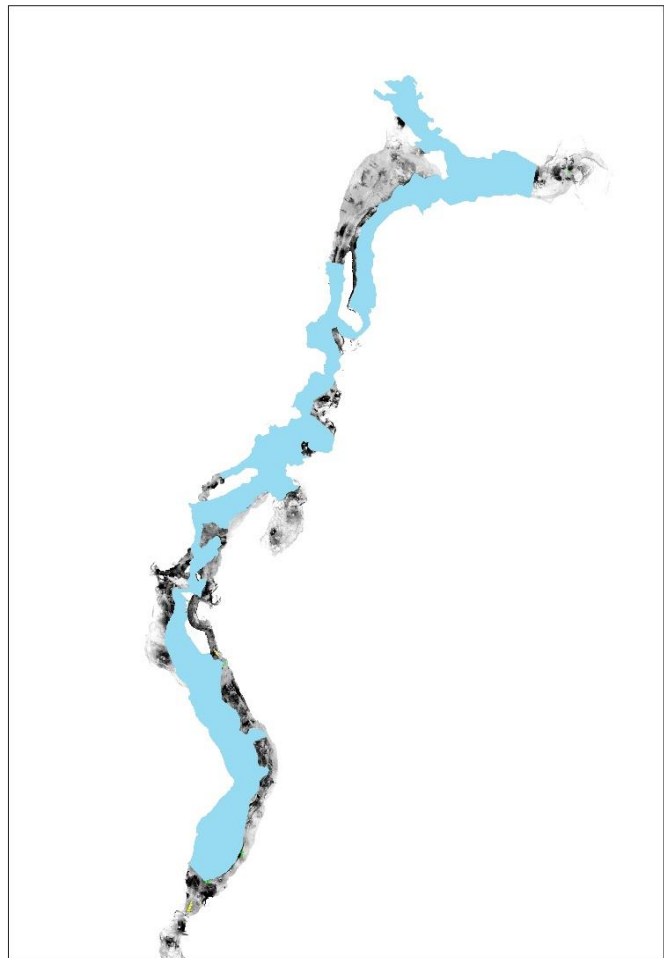


Figure 10. Digitalized study area with rectified laser scanned data

2.2 Basic Principles Of GPR Data Acquisition

2.2.1 GPR systems

Ground penetrating radar (GPR) has been widely used by the geographical community on the shallow subsurface investigations since the 1970s (LB Conyers, 1997). As a geophysical method that can detect the spatial features of near-surface, radar pulses from transmitting antennas propagate ground surface, reflected off subsurface, buried objectives, soil units, and detect the echo with distinctive characteristics and the time interval with the radar pulse by receiving antennas, as demonstrated in *Figure 2.7*. Comparing to the traditional subsurface measurement method like drilling, often acquires limited information from scattered sampling points, GPR has a significant advantage of less time consuming and less expensive, especially under some circumstances that traditional invasive techniques cannot be implemented due to the limitation of the environments.

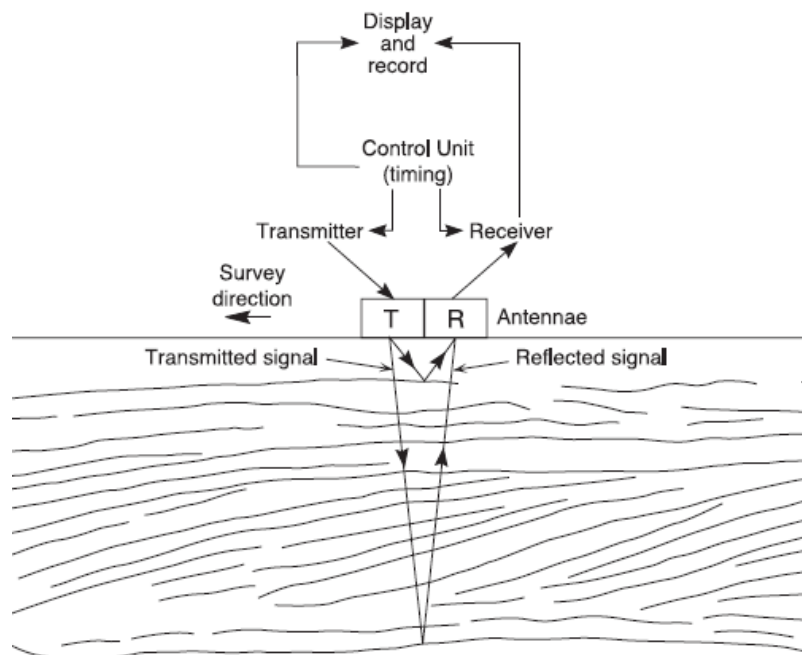


Figure 11. GPR data acquisition (A. Neal, 2004)

While data is being collected, a horizontally sequential reflection traces are being recorded to build up a radar reflection profile. A single trace is interpolated from the high-frequency radar pulse emitted energy which is transmitted to the ground surface. The velocity of the EM wave that sent downwards varies as the EM wave interacts with different mediums with various electrical properties. The abrupt change of the EM wave energy is marked on the

reflected signal which can be received by the receiving antenna, the abrupt changes on transmitting energy can be detected by the amplitudes of the wave (*Figure 12*). In the meantime, the time interval between two transmitting is recorded as two-way travel time; the measuring time unit is nanosecond (10^{-9} s).

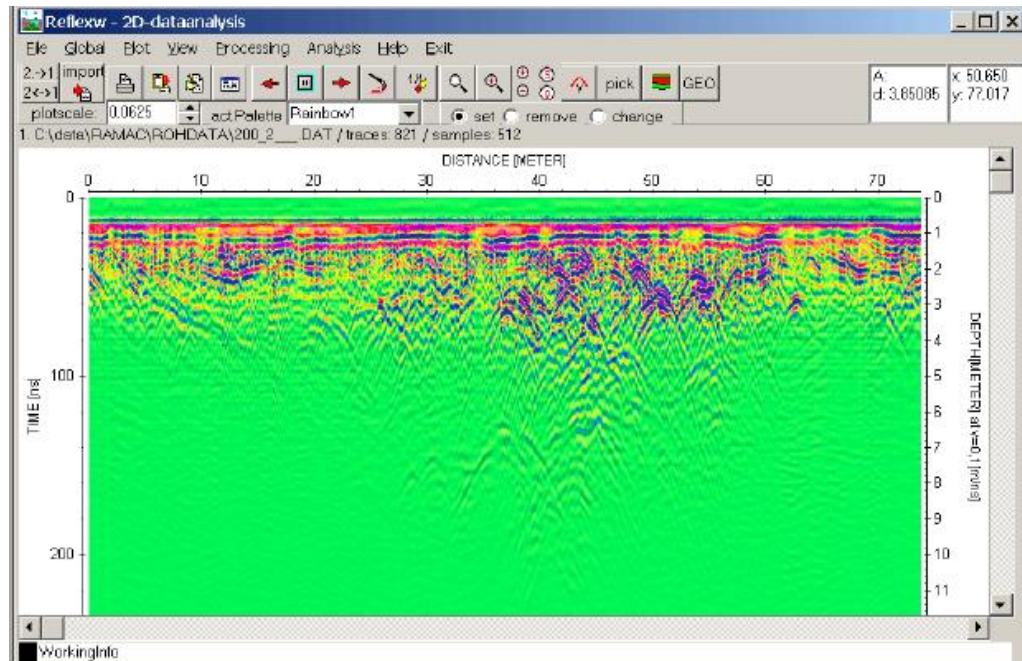


Figure 12. Display of Amplitude Difference of Raw GPR data on Reflexw Software

Before the invention of GPR, seismic reflection and seismic refraction were the most commonly used techniques for shallow subsurface detecting, which cannot provide a satisfactory vertical resolution for practical uses (A. Neal, 2004). GPR system's origins lie in research carried out in the early 1920s by German scientists trying to patent techniques to investigate the nature of various buried features (Daniles, 1996; Reynolds, 1997), during which electromagnetic waves were first used. From the 1970s, the researchers noticed that the GPR systems are advantageous for recording the subsurface features (typically shallower than 50 meters). However, with the earliest generations of GPR systems, the raw subsurface reflection data allows little pre-processing and post-processing.

The commercial availability of GPR systems started in the 1980s, the data collection became feasible (Annan and Davis, 1992). With the development of modern digital systems, GPR data's collecting, recording, interpreting, and displaying have been dramatically simplified and accelerated. Due to the seismic reflection and EM wave reflection have many similarities, the seismic reflection processing technologies can be used for GPR data as well (Fisher et al.,

1992a; Maijala 1992; Rees and Glover, 1992; Young et al., 1995; Fisher et al., 1996; Annan, 1999; Pipan et al., 1999).

Common-source or common-receiver surveys are rarely performed in GPR studies (A. Neal, 2004). In this study, the 3D GPR system RIS MF Hi-Mod (*Figure 13*) was used, it has a multi-frequency data fusion of data from 200 and 600 MHz antennas. The conductivity of frozen water body allows electromagnet waves to propagate and reflect. Additional, this system offers following features:

- Consolidated complete procedure from field acquisition to the final output (maps or CAD or GIS)
- Mechanical structure for all urban environments and terrains
- Automatic target recognition, automatic tools help the operator locate pipes and cables
- 2D and 3D tomography: optimized tomography for immediate visualization of pipes and cables
- Multi-frequency data fusion: automatic fusion of data from 200 and 600 MHz antennas
- Automatic transfer to CAD/GIS: localized pipes and cables automatically transferred to CAD or GIS maps.



Figure 13. Installation of the RIS MF Hi-Mod GPR system

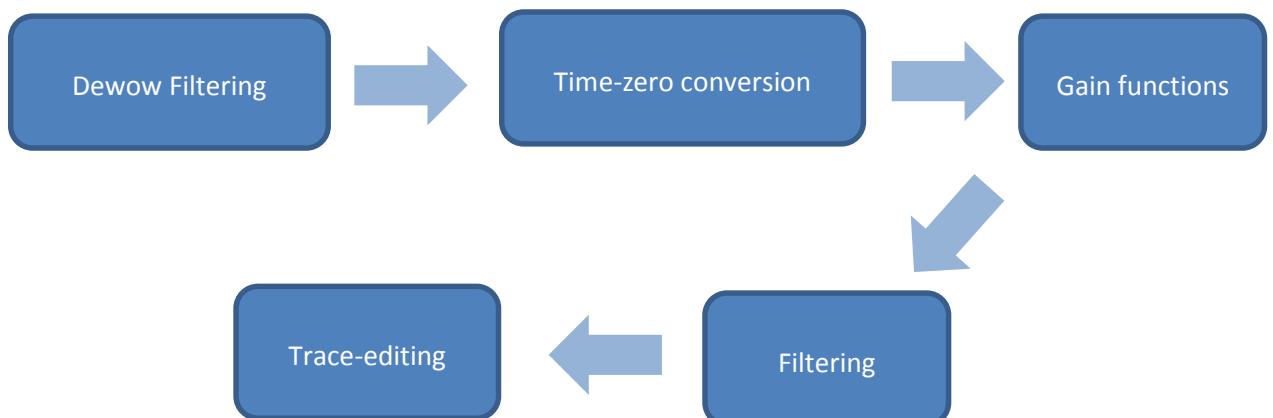
2.2.2 GPR datasets

The raw 3D datasets acquired by a GPR system usually contain geometrical information of the profile, include coordinate parameters as XStart, XEnd, YStart, YEnd, ZStart, ZEnd, time and comment specification as TimeDimension, time increment, sample number, trace number, trace marks. Additionally, geographical coordinates provided by internal global positioning system also included, however, GPS coordinate is not applicable in this study since GPS signal could not reach inside of the ice cave.

From the 20th April 2017 to the 23rd April 2017, 143 datasets have been collected, respected to 143 survey lines, all of the measurements were obtained from the 200MHz antenna since considerable depth was expected. The recording parameters were set to 2048 samples per scan and 16bits per sample. Due to the complex ice-dominant with distinct slope environment inside the cave, the profiles were obtained by languid hand- towing. And some of the profiles were even obtained by pulling the radar upwards or downwards to the slope. Thus, the recording speed is about 0.5m per second averagely.

2.3 GPR Data Pre-Processing

The standard raw GPR reflection data is a two-dimensional profile with two axes. Usually, the X axis stands for the measured distance on the ground, Y axis stands for the vertical depth. One profile is a collection of a stack of reflection traces, obtained as the antennas moved along a transect. The raw GPR data inherent the limitations from seismic surveying, therefore signal processing methods, usually dewow filtering, time-zero conversion, data correction, and trace editing. In practical applications, these pre-processing usually are required before further interpretation. A primary workflow for GPR data pre-processing in this study is shown below.



2.3.1 Dewow Filtering

The wow effect of the raw GPR data is a unique aspect of GPR data arises from the proximity of receiver to the transmitter (Harry M. Jol, 2009). The low-frequency energy associated with electrostatic and inductive fields near the transmitter decay rapidly with distance. A slowly time-varying component to the measured field data caused by this low-frequency energy, on the Y-Axis of the data, a time shift showed on the received signal to bow up or down (*Figure 14*).

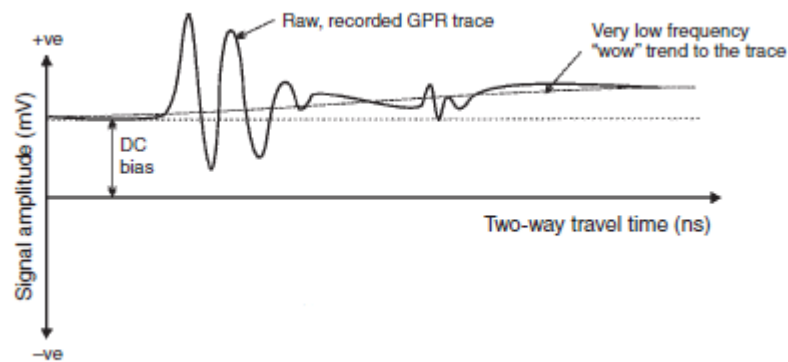


Figure 14. The wow effect on GPR signal (Harry M. Jol, 2009)

Firstly, it is inevitably for GPR raw data to have wow noise as electromagnetic data, before the accurate result has been produced, the wow noise must be removed. Also, be recognized as primary DC signal component, or DC bias, the low-frequency signal trend to subsequently decay (Dougherty et al., 1994). The “Wow” noise is caused by the swamping or saturation of the recorded signal by early arrivals (i.e., ground/air wave – Annan, 1993) or inductive cou-

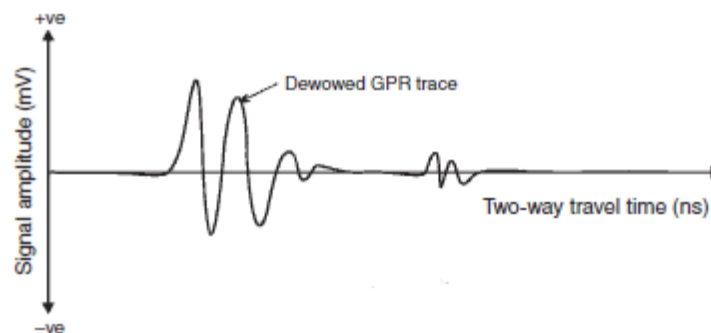


Figure 15. GPR signal after dewow filtering (Harry M. Jol, 2009)

pling effects. Which requires the subtraction of the DC bias from the signal and the application of an optimized, low-cut or median filter for effective correction (Gerlitz et al., 1993; Fisher et al., 1994). Dewowing is a vital step as it reduces the data to a mean zero level and, therefore, allows positive-negative colour filling to be used in the recorded traces (Harry M. Jol, 2009) (*Figure 2.10*).

In this study, a manual dewow correction is required, with the processing software Reflexw, the subtract-mean filter is used to normalize the data. With this option, a running mean value is calculated for each value of each trace. This running mean is subtracted from the central point. The filter parameter the time window is set to 4 nanoseconds for calculating the running mean value.

2.3.2 Time-zero correction

To correct the misalignment of the first reflection break that occurs in the radar profiles, GPR data processing software often contains packages for realigning the profiles, which works by physically moving individual traces upwards or downwards by the required amount of the two-way reflection time. A threshold is required to identify the first break.

A time-zero drift can be caused by thermal drift, electronic instability, cable length differences, and variations in antenna airgap, which can cause “jumps” in the air/ground wavelet first arrival time (Olhoeft, 2000; Nobes, 1999; Young et al., 1995). Usually, an automatically adjusting method is applied in the GPR data processing software since time-zero variations may happen.

In this study, the first pulses echo back from the ice surfaces as well as the radar shell itself. These reflections need to be eliminated, to ensure that the time-zero correction produces results that are consistent across the traces. The threshold is set to be 18 nanoseconds to move the traces upwards (*Figure 16*). This process step is regarded as the minimum required method for viewing the data in a normalized form.

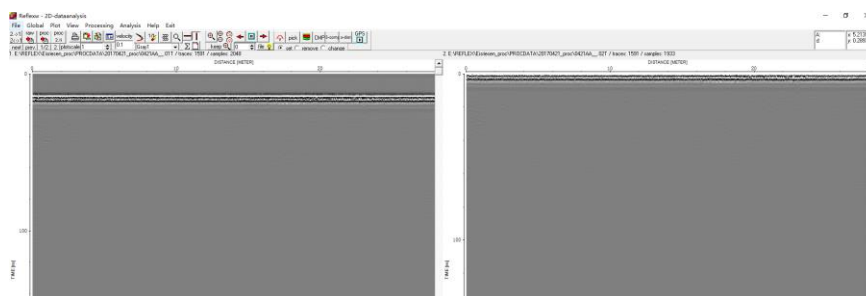


Figure 16. Example of time-zero correction in 0421AA GPR data section

2.3.3 Gain functions

For further application and interpretation, optimized gain functions need to be applied to the GPR sections, which improve the visual form of the data by altering the data structure like relative amplitudes, phase relationships. Therefore, it is essential that's the effects of the gain functions is understood before they are applied, and the data are treated with care when interpreting (Annan, 1999). Filters tend to optimize the shape of individual traces through mathematical manipulation, enhancing or eliminating specific features. For enhancing the appearances of the temporally later reflection arrivals, temporal gains are required. There are also gains, which are usually spatial filters, work horizontally on the positions of adjacent traces.

There are different temporal gain methods, like constant gain, exponential gain, SEC, AGC. In this study, the user-defined gain function is used to enhance the subsurface boundaries. However, the operator bias is inevitable since the gain function amplify both noise and coherent signals by altering the data directly.

SEC function, also known as energy decay function, which provides an automatic correction of the amplitude anamorphous errors of the signal caused by the loss of the energy from the geometrical spreading effect of the propagation wave front. Furthermore, the material attenuation losses (dB/m) can also be included as an additional factor in the function, which usually requires an accurate attenuation for processing. Such parameters can be hard to obtain even with CMP surveys, as a solution, a priori or a "best guess" are always used instead. As a key factor, spreading and exponential compensational gains to retain the relative amplitude information are crucial during the signal interpreting.

AGC is an automatic gain function applied to individual traces. Based on the difference between the mean amplitude of the signal in a particular time window and the maximum amplitude of the signal of a trace as a whole (Harry M. Jol, 2009). For enhancing the in-depth, weak features on the traces, a processing window size needs to be defined, typically range from 3% of the total sample length up to 25% of the propagating wavelet length (Annan, 1999). An inappropriate set of the window size can cause either enhanced noises or the "shadow zone" caused by the reduced amplitude generated at the rear of the reflections.

User-defined gain function, also known as constant, linear or exponential gains. The user defines the function directly by changing the exponent (dB/m) or the linear, exponential parameters. In other cases, the mathematical or multiplication operator can be defined by the system automatically. In general, the user-defined retain some relative amplitude information but how much depends on the type and mode of the function applied (Harry M. Jol, 2009).

In the example of *figure 16*, a linear gain and an exponent parameter were set to enhance the later arrivals of the reflected waves. The comparison between a data set before and after gain function filtered is showed in *figure 17*.

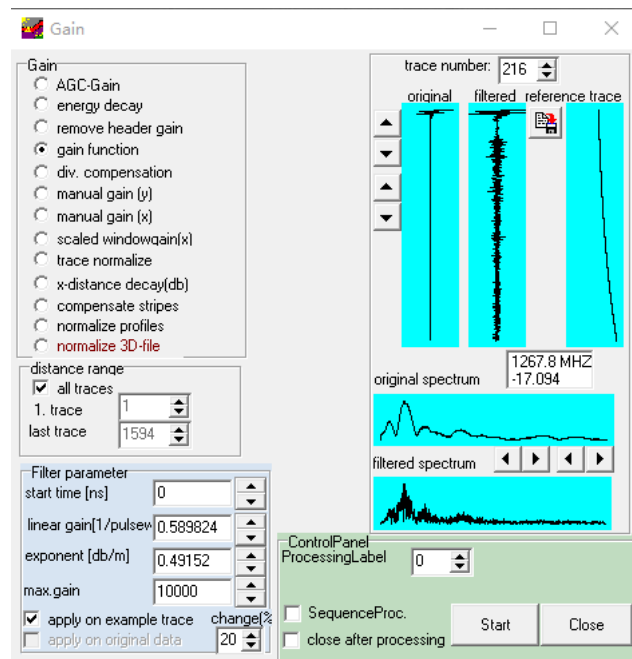


Figure 18. Example of setting a user-defined deep feature enhancement gain function

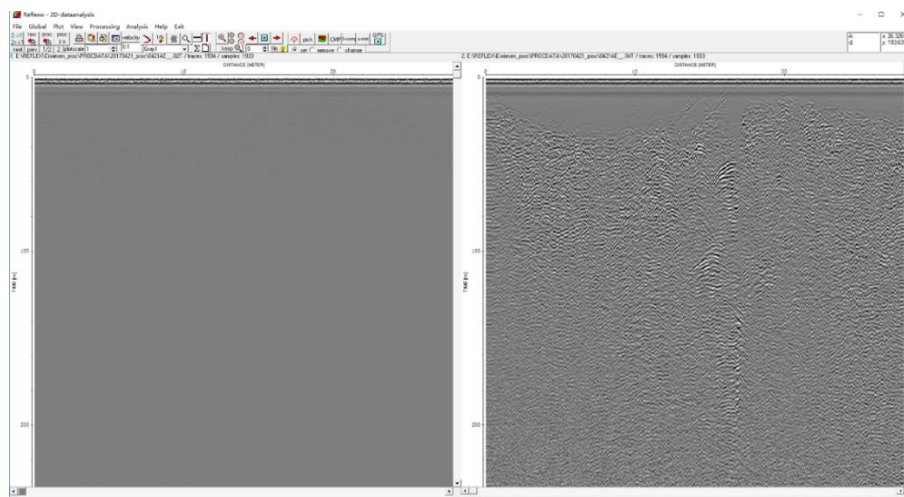


Figure 17. Example of user-defined gain function applied on dataset 0421AE

Filtering methods are applied to eliminate the system or manual errors, for examples, the removal of high-frequency “speckle” noise from radio transmissions (Olhoeft, 2000) or the striping effect from antenna ringing (Lehmann et al., 1996). Also, filtering can enhance certain features through mathematical manipulation. Inherited from seismic signal processing methods, there are many different types of filtering methods can apply to GPR data, from simple band-pass filters to sophisticated domain and transform filters (Lehmann et al., 1996; Pipan et al., 1999; Young and Sun, 1999).

Under the circumstance that the post-gain data is fully understood, the filters can be applied. In this study, only the ice-ground boundary is interested, which can already be recognized after gain. Therefore the filters can be applied post-gain to emphasizing the median difference by suppressing the noises.

In general, filters are defined as two basic types; temporal filters act vertically on the time dimension apply on individual traces sequentially. Spatial filters act horizontally on the spatial dimension use adjacent traces. In the Reflexw software, many simple 1D-filtering on both dimensions methods are provided:

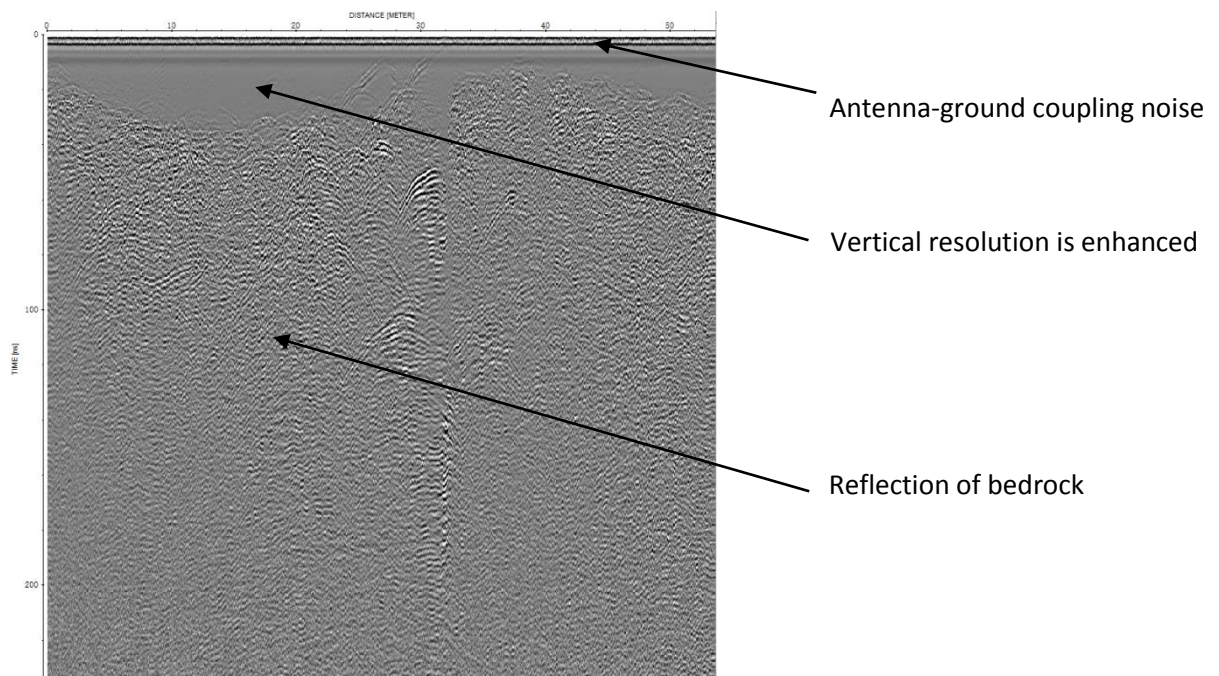
Simple mean filter, a temporal filter smooths the data by taking the mean of the data across a specified time window. Usually used for removing excessive high-frequency noise from the data, e.g., the radio frequency interference from mobile communicating devices; Simple median filter. For the power spike removal and cleaning up filters by taking the median value of the data within a pre-defined processing window; Low- or high-pass filters, which allows the data component within specified frequency domains to pass the filter to eliminate the noise exists in high- or low-frequency domains.

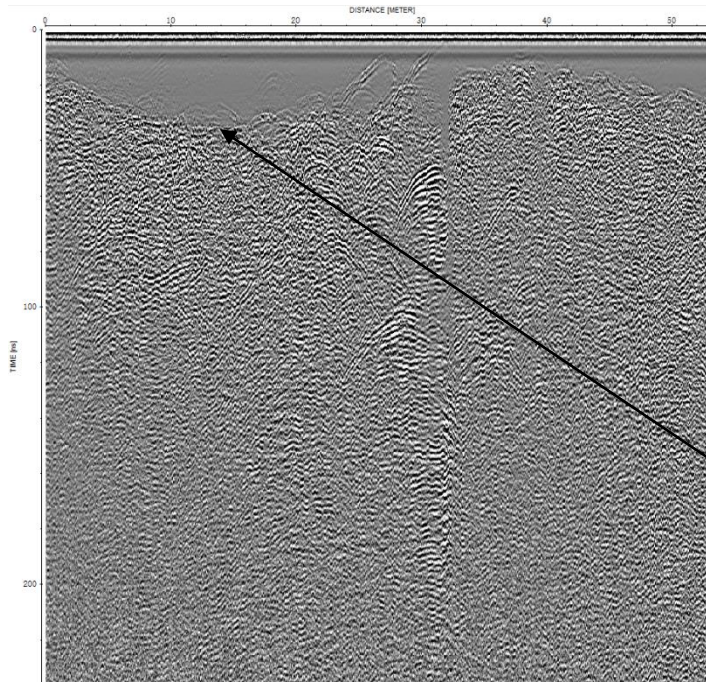
For spatial filters, simple running average filter, average subtraction, background removal and spatial band, high- low-pass filters are provided. Combing to temporal 1D-filters, advanced 2D filters are produced. Which operate on the data in both temporal and spatial dimensions simultaneously. For examples, t-x average and t-x median filters for general noise removal and Frequency-wavenumber (FK) filter, an advanced 2D filter combine time-space and band-pass filters.

In many cases, practitioners usually use a simple 2D running average filter, which smooths data horizontally and emphasizes flat-lying reflection layers. However, the smoothing factor of this filter reduces horizontal resolution rapidly, and distort important dipping reflections.

Thus, unaffected 2D running average filter is not applicable in this study since the reduction of the resolution on the ice-sediment boundary.

In this study, involved filters are not necessary, since only the impulse response of the subsurface needed. Also, the individual internal layers of the study area can be assumed to have unified EM wave propagation velocities with non-scatter energy. In these terms, deconvolution is an ideal signal processing method. Act in the temporal dimension as an inverse filtering process, deconvolution enhances the sectional resolution by compressing the recorded GPR wavelet into a narrow, distinct form (Yilmaz, 2001). It can also be recognized as a filter that removes the effect of the source wavelet from the recorded data (Neves et al., 1996), leaves the impulse response of subsurface layers only. However, as an integrated signal processing method from the seismic analysis, there is a very restricting assumption on the subsurface is more complicated and the propagating GPR wavelet is mixed phase, non-stationary and non-planar, with a spatial complexity. Thus, deconvolution has limited usefulness in the well-defined and less-complex subsurface. However, the effectiveness of deconvolution can be proven in the following example (*figure 19*), while the propagation velocity variation between the ice layer and the bedrock is significant.





The upper part of this figure is a profile after basic process, dewow filtering and time-zero correction. With user-defined gains applied. The lower part is the same processed profile with deconvolution applied. The subsurface impulse response is significantly enhanced.

The boundary between subsurface layers is strongly enhanced

Figure 19. Example of deconvolution filter applied on 200MHz GPR data (0421AE)

2.3.4 Trace editing

With a large volume of data, it is inevitable that errors occur. To maintain the sequential and spatial correctness of the data, traces are needed to be re-arranged and sorted, which can be achieved by trace editing. The editing methods include trace reversing, merging, splicing and eliminating. In this study, the raw dataset has noticeable trace redundancy due to the occasional stops of the antenna while scanning. Thus trace elimination is necessary for the quality of the dataset, also a requirement of effective data maintenance.

Moreover, the incorrect of recording parameter occurred in the data header files, mostly the profile length. Therefore, the header file of simple profile needs to be checked and edited individually.

2.4 Time-Depth Conversion of GPR Data

So far, the pre-processing steps used in this study operate only in the time domain. The relation to the vertical spatial domain, the depth have not been established. To interpret the scan profiles to actual readable spatial data with depth axis, time-depth conversion is a crucial step. Due to the traveling through of reflected impulse causes energy loss, the signal and

space displacement of subsurface features on the recorded signal is also inevitable. Thus, data migration is necessary for spatial correcting, also giving the reflect pulses geometric features.

2.4.1 Propagation velocity analysis

GPR data is recorded on a fixed and invariant time base (A. Neal, 2004). An estimation of depth can only be obtained with information of the radar wave propagation velocity. With the velocity parameters, the depths of the different subsurface can be calculated by a simple linear conversion equation.

However, significant changes in velocity can occur vertically due to different subsurface properties. The accurate estimate of the different subsurface velocity can be obtained through ground investigation or common midpoint surveys (CMP). For the cave ice of the ERW cave, a ground investigation has been completed by former researches, for an investigation depth of 5 meters and an electromagnetic wave of 0.167 m/ns the Fresnel zone has a diameter of 2.9m (200MHz) (H.Hausmann, M. Behm, 2011). The bedrock is regarded as granite with a velocity of 0.13m/ns (Hubbard and Glasser, 2005). Typical electrical properties of common subsurface materials are listed in *Table 2.1*

The propagation velocity of radar waves through a certain material can be given by:

$$V = \frac{c}{\sqrt{(\varepsilon/2)[(1 + P^2) + 1]}}$$

Where c is the speed of the radar wave in vacuum space (e.g., the travel speed of light, $c = 3.0 \times 10^8 \text{ ms}^{-1}$); ε is relative electrical permittivity; P as the loss factor. Due to the propagation of radar wave causes a significant loss of wave power, defined as $P = \sigma\omega\varepsilon$ where σ is electrical conductivity, ω is angular frequency ($= 2\pi f$, where f is the frequency of the radar wave). Theoretically, the velocity of radar wave in ice will be slightly higher in relatively cold, dry ice (Hubbard and Glasser, 2005). The cave ice in the ERW cave can be regarded as the natural ice made of fresh water, the propagation velocity of ice, as 0.167 m ns^{-1} is applicable.

Material	Relative electrical per-mittivity	Electrical conductivity (mSm^{-1})	Velocity (m ns^{-1})	Attenuation (dB m^{-1})
Air	1	0	0,30	0
Distilled water	80	0,01	0,033	0,002
Fresh water	80	0,5	0,033	0,1
Salt water	80	3000	0,01	1000
Dry sand	3 - 5	0,01	0,15	0,01
Saturated water	20 - 30	0,1 – 1,0	0,06	0,03 – 0,3
Silt	5 - 30	1 – 100	0,07	1 – 100
Clay	5 - 40	2 – 1000	0,06	1 – 300
Granite	4 - 6	0,01 – 1	0,13	0,01- 1
Ice	3 - 4	0,01	0,167	0,01

Table 2, typical electrical properties of common subsurface materials (Hubbard and Glasser, 2005)

2.4.2 Data Migration

After the basic processing of GPR data, here comes the final step of GPR data preparation. To be recognized as the most controversial technology in GPR data analysis, migration is very effective for enhancing the section resolution as well as giving the subsurface more spatially realistic. The same as data deconvolution, the migration technology is also inherited from seismic signal processing methods. Data migration has been successfully used for relatively uniform environments, like glacial research. Migration methods include Kirchhoff migration (Moran et al., 1998), F-K migration (Fisher et al., 1994), and reverse time migration (Fisher et al., 1992a, 1999b; Sun and Young, 1995; Meats, 1996). Kirchhoff migration is ideal for radiation patterns and interface reflection polarization (Moran et al., 1998; Van Gestel and Stoffa, 2000). Comparing to other technologies, for examples, F-K migration, mostly used for landmine detecting (Song et al., 2006). Frequency domain migration modified for loss soils (Ding and Wang, 2004; Streich et al., 2007). The Kirchhoff migration is the ideal migration method for this research.

Despite the differences of the mentioned migration technologies, all the data migration were designed to reconstruct the GPR reflection, as converting the impulse waves to the objects. Giving the sections a spatial accuracy through a subsurface velocity model. The methodology of data migration can be separate from diffraction and reflections processing. For the diffractions, the migration attempts to correct both the position and amplitude of the recorded signal on the diffraction hyperbola by reconstructing the wavelet at the target point source.

The algorithm tries to match an ideal hyperbolic function to the diffraction form, or by building a model on the space movement of the trace, to relocate the traces into the correct po-

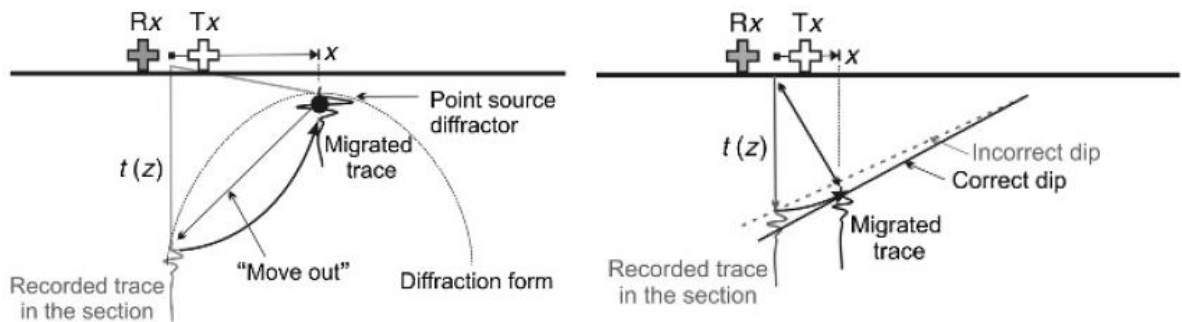


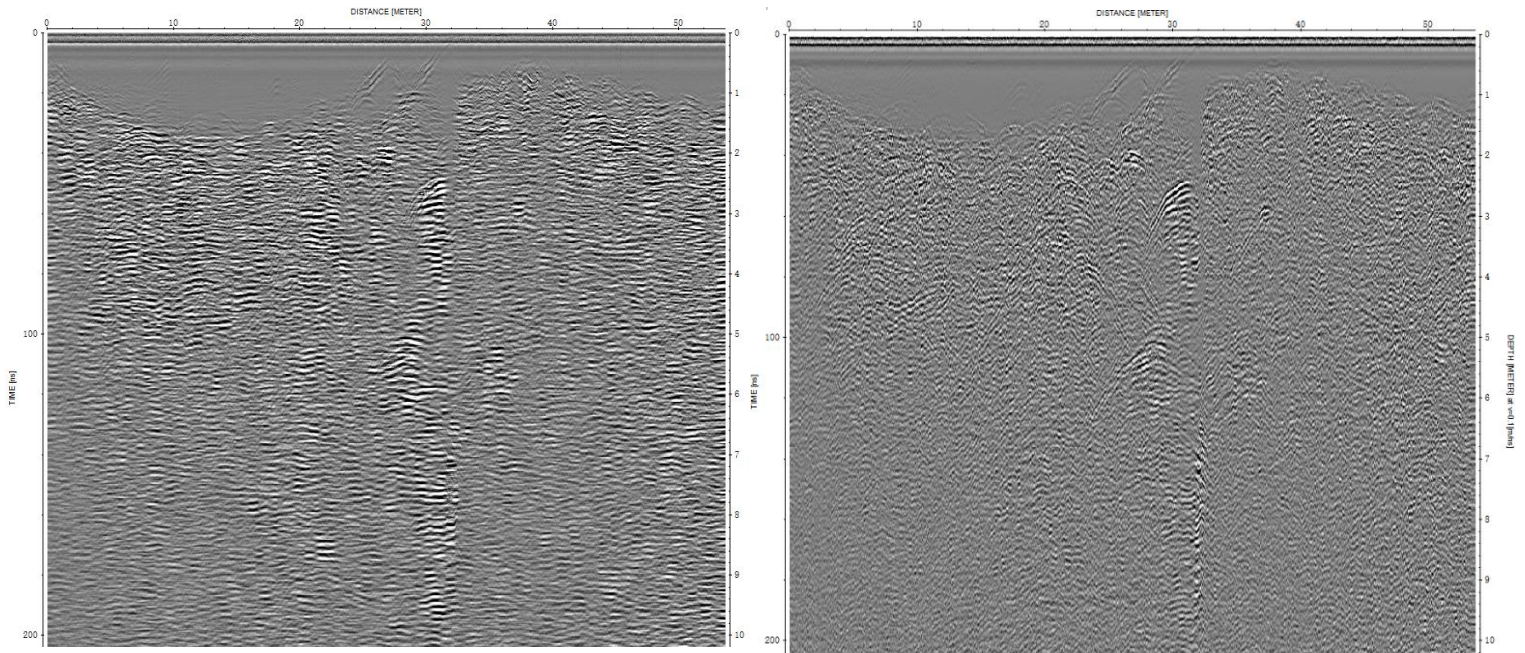
Figure 20, signal position correcting by diffraction hyperbola and corrected trace dips

sition. An accurate velocity-depth model is needed to calculate the relocating parameters like horizontal distance, depth or time-domain distance. Reflection migration, different from the diffraction migration, correcting the position of the reflectors by the correct dip of the recorded reflection. Because the recorded signal is plotted beneath the mid-point of the antenna pair. In fact, the reflection signal located “ahead” of the antenna. Thus, horizontal distance and vertical distance are needed for the dip modelling (*Figure 20*).

Data migration is always limited by the complexity of the actual environments. A Neal (2009) generated the limitation of GPR data migration as follows:

- The velocity structure of the subsurface must be known (or accurately estimated), and the stratigraphy is constructed of laterally invariant, constant velocity layers.
- The source is spatially uniform and propagates spherically.
- The far-field conditions of a radial, uniformly propagating scalar field are assumed.
- Data are collected in normal incidence or monostatic mode – i.e., there is no antenna separation.
- No dispersion or attenuation is allowed – i.e., the materials are lossless and have frequency-independent properties.

In the Reflexw software, a common midpoint surveys (CMP) or hyperbola matching velocity model is necessary for data migration. While building a CMP model, detailed information on subsurface propagation velocity is necessary. However, no matter how comprehensive the velocity information is, it is always impossible to rebuild the real environment. Thus, the errors will always occur in migrated data. It is recognized that the errors more than 5%-10% will cause blurring, defocusing of the target features and the misalignment of reflectors (Yilmaz, 2001).

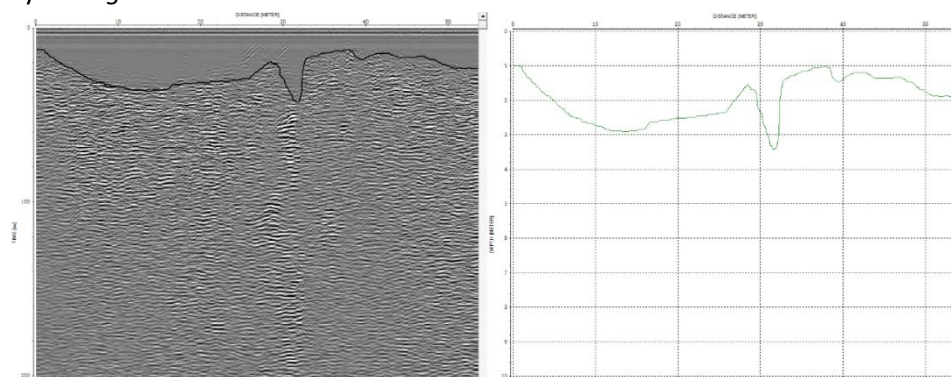
*Migrated**Unmigrated***Figure 21.** The comparison between unmigrated data and migrated data

For the cave ice investigation, Kirchhoff migration method would be ideal, since, in this method, only vertical velocity variations accounted. The Kirchhoff migration corrects the amplitude and phase before summing amplitudes along diffraction hyperbola.

A successful migration can significantly improve the spatial resolution power of GPR data, the data interpreting, as a result, would be easier in comparison. An example of the comparison between the pre-migration data and the post-migration data is shown in *Figure 21*.

2.4.3 Layer analysis

After data migration, the depth of ice layer has already been known, and for the effectiveness of the sampling in next steps, a continuous layer is necessary to describe the bottom of the ice body. As *Figure 22*.

**Figure 22.** Estimation of ice-bedrock boundary layer

2.5 Elevation Extraction From Laser Scanned Dataset

In the raw laser scanning dataset obtained by Rico Beckert (2013) with FARO FOCUS 120 laser scanner, the field “altimeterCurrentAltitude” recorded the reading on the altitude meter of single scan station while doing scans. The elevation values used in this thesis were from this dataset.

3 METHODOLOGY

After going through the data preparation steps illustrated in the last chapter, this chapter will focus on the detailed solutions to the research questions and the ideas behind these solutions. In general, the comprehensive workflow of this these research can be divided into five parts as follows: GPR data Pre-Preparation, Time-Depth Conversion, Depth Information Extraction, LiDAR Data Feature Extraction, and Data combination and Mapping (*Figure 3.1*). As data preparation has been integrally described in chapter 2, this chapter will introduce the methodology of GPR surveying, includes the accuracy assessment of the data, the basic ideas of feature point extraction, as well as the interpolation method of the depth points on the digitalized ice surface.

Moreover, the cartographic design methodologies of the ice basement maps are included. As results, a series of thematic maps focus on the full ice thickness will be produced. In this map series, ice thickness will be present by classic contour lines, with the cave outline obtained from the orthoimage from the laser surveys. With the contour lines, not only the ice thickness, as well the ice basement can be well illustrated. There will be another map focusing on the efficiency of illustrating, based on the colour rendering for different thickness of the ice surface, the readers of this map will have a quick idea on the distribution of the ice thickness. The base map will be the orthoimage from laser survey to show the terrain roughness inside the ERW cave.

While the maps were being produced, the positions of some geometrical features such as breccia and ice fall/ice column were inherited from the cave map that mentioned in the first chapter.

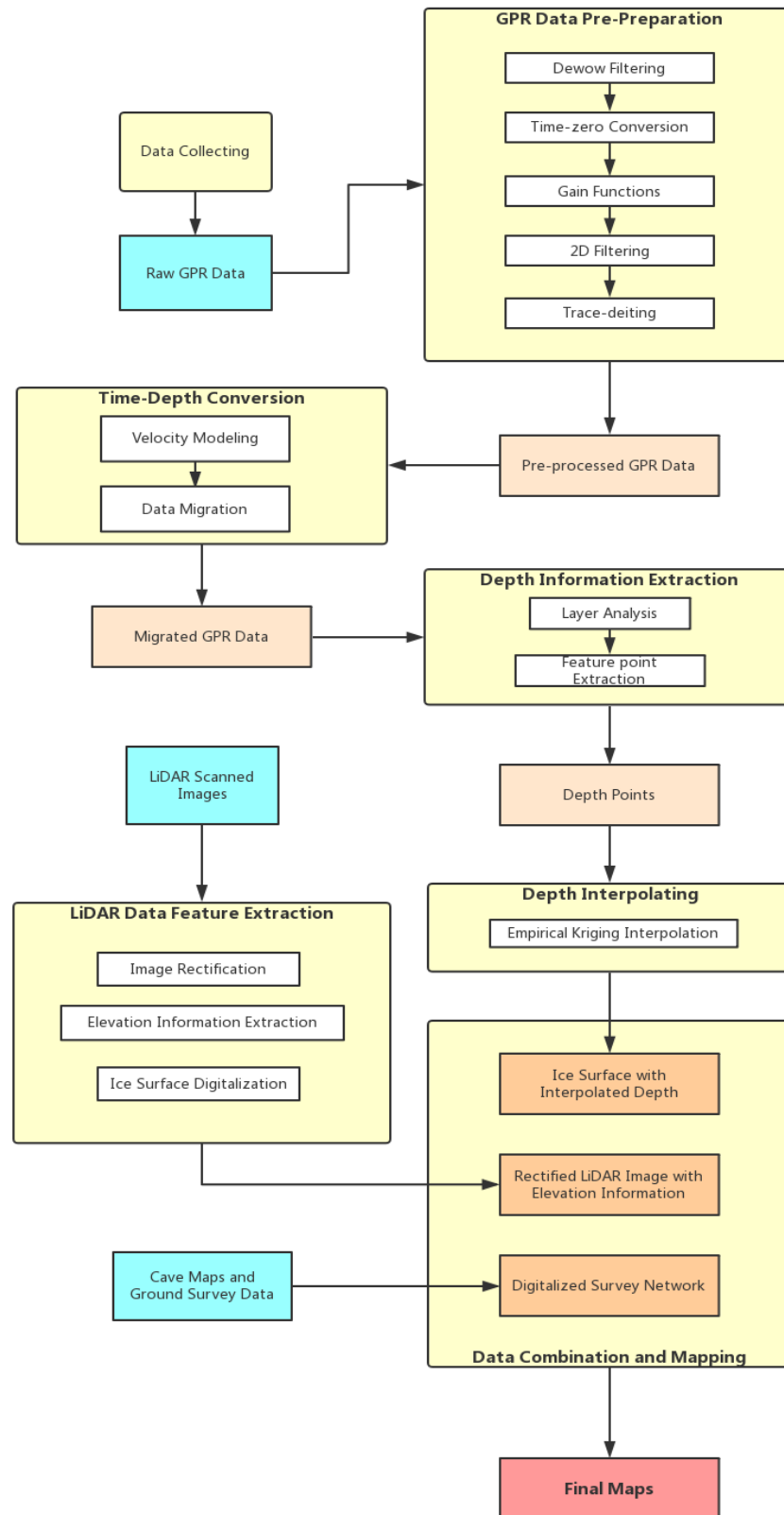


Figure 23. Methodology to ice basement mapping with GPR survey data

3.1 Electromagnetic Features of Subject and Radar Wave

As demonstrated in the second chapter (*Figure 11*), ground penetrating radar obtains the information of subsurface by the feature of electromagnetic waves reflection. For the EM wave field, there are vital factors which are exploited in the methodology of GPR, like the propagation velocity, v , attenuation, α , and EM impedance, Z (Annan, 2003). While the EM wave travels through a single medium with a fixed permittivity, conductivity, and permeability, attenuation occurs. The attenuation results in the uniqueness of the amplitude and velocity for a specific medium. The properties can be described with the common properties and an estimated sinusoidal time variation.

The behavior of all the waves can be similar, so to say in the low-frequency domain (0.001MHz to 10MHz), wave properties depend on $\sqrt{2\pi f}$, f stands for frequency, the diffusive act of the wave field is evident. In high-frequency domain (from 10MHz), the wave behavior is a frequency-independent. For GPR surveying, the high-frequency domain characteristics are the most important.

Since in the most used frequencies of GPR, all frequency components travel at the same velocity, also attenuated by the same law in a uniformed medium, the velocity, attenuation, and impedance can be expressed as:

$$v = \frac{1}{\sqrt{\varepsilon \cdot \mu}}$$

$$\alpha = \sqrt{\frac{\mu}{\varepsilon}} \cdot \frac{\sigma}{2}$$

$$Z = \sqrt{\frac{\mu}{\varepsilon}}$$

In the first equation, ε stands for dielectric permittivity, which characterizes displacement of charge constrained in a material structure to the presence of an electric field. Magnetic permeability μ is a characteristic that expresses how intrinsic atomic and molecular magnetic moments respond to an EM field. The σ electrical conductivity describes free charge movement when an electric field is present. These three electrical properties can characterize the behavior while a specific material exposes in electric fields, and always can be determined by laboratory analysis for a pure material.

With the electromagnetic properties, the behaviors of GPR wave can be easily foreseen. Since ground penetrating radars are usually used to investigate subsurface features through electrical low-loss materials, for instance, if the electrical conductivity σ is zero, the impulse would penetrate to a considerable depth. And the dielectric permittivity ϵ constrains the propagation velocity of the wave.

In the natural environment, the subject usually shows a complex mixture of different materials, but in the bigger picture, the electrical properties mostly depend on the presence and the amount of water in the medium in the 10 – 1000MHz domain. The observed behaviors of general materials were described as follows in the previous researches (Topp et al., 1980) (Aeche, 1942):

- Bulk minerals and aggregates in mixtures generally are good dielectric insulators. They typically have a permittivity in the range of 3-8 (depending on mineralogy and compaction) and are usually insulating with virtually zero conductivity.
- Soils, rocks, and construction materials have empty space between the grains (pore space) available to be filled with air, water, or other material.
- Water is by far the most polarizable, naturally occurring material.
- Water in the pore space normally contains ions, and the water electrical conductivity associated with ion mobility is often the dominant factor in determining bulk material electrical conductivity. Resulting soil and rock conductivities are typically in the 1–1000 mS m⁻¹ range.
- Since water is invariably present in the pore space of natural (geologic) materials, except in such unique situations where vacuum drying or some other mechanism assures the total absence of water, it has a dominant effect on electrical properties.

As both the electrical properties of the subjects and the radar waves depend on the recorded signal of a GPR, the wave behavior is on the same level of importance to the methodology of GPR surveying. Once the impulse is emitted by the radar and reaches the surface of a material, or an interface between two different materials, the wave will conduct three main behaviors: reflection, refraction and transmit, as described in *Figure 24*.

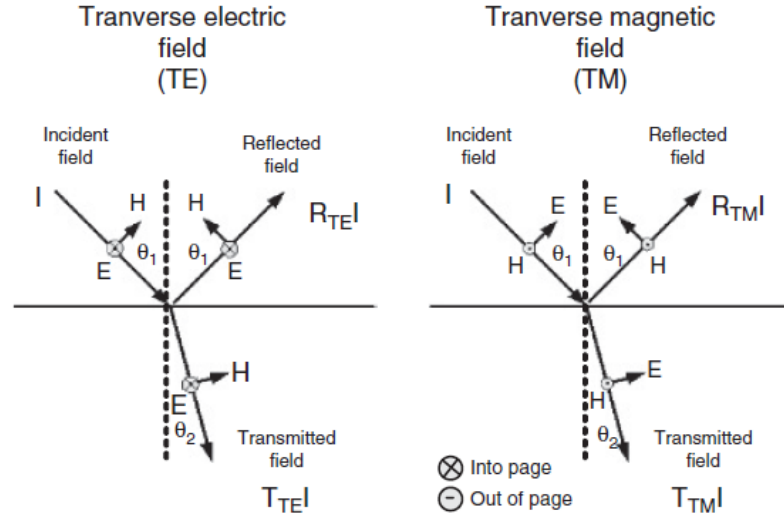


Figure 24. Quantificational model of electromagnetic wave between two materials (A. Neal, 2009)

With the Snell's law, the direction of the wave changes while travelling through the interface between different mediums, the transmitting energy is also separated into two components, TE (transverse electric field) and TM (transverse magnetic field) (Annan, 1973).

For ground penetrating radars, a quantificational expression of reflected energy is the key factor, which can be defined by the following formulas:

$$R_{TE} = \frac{Y_1 \cdot \cos \theta_1 - Y_2 \cdot \cos \theta_2}{Y_1 \cdot \cos \theta_1 + Y_2 \cdot \cos \theta_2}$$

$$R_{TM} = \frac{Z_1 \cdot \cos \theta_1 - Z_2 \cdot \cos \theta_2}{Z_1 \cdot \cos \theta_1 + Z_2 \cdot \cos \theta_2}$$

The Z_i and Y_i stand for the impedances and admittances of the i th material. Under an ideal circumstance, $\theta_1 = \theta_2 = 0$, the TE and TM reflection coefficients become identical.

3.2 Accuracy Assessment

The resolution power for non-contact sensors is a crucial feature. The resolution indicates the limit of certainty in determining the position and the geometrical attributes of a target (such as shape, size, and thickness) (Annan, 1999). The explanation of the resolving power of GPR systems is inherited from seismic measuring, includes two factors, which are horizontal resolution and vertical resolution (Figure 3.2). For the horizontal resolution, the ability to resolve two firmly positioned features (Knapp, 1990). Respect to the horizontal resolution, the vertical resolution defines the resolving power of the depth domain, which depends on

the wavelength of the impulse from the antenna. The wavelength can be calculated as follows:

$$\lambda = \frac{v}{f}$$

In this equation λ is the wavelength, v is the propagation velocity, while f is the frequency. While assessing the resolving power of a GPR, the return signal received by the receiving antenna is mostly used. Since during the propagation of the signal, the energy losses will reflect the change of frequencies, usually, the receivers receive signals with a relatively lower frequency. A higher frequency is preferentially attenuated as waves propagate through the earth, resulting in a longer average wavelength (Jol, 1995; Bano, 1996).

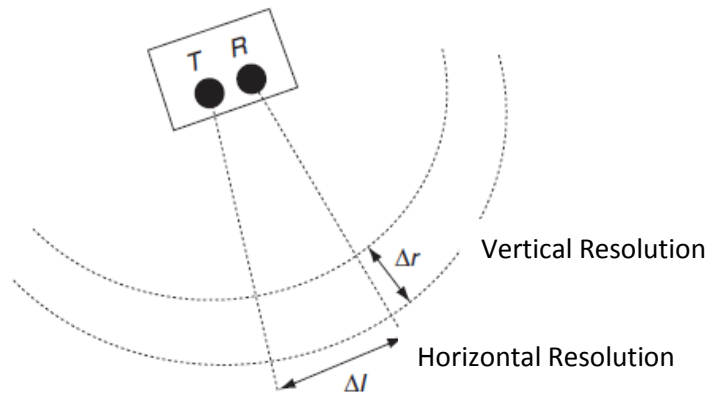


Figure 25. Two resolutions of GPR system

From the wave theory, the best vertical resolution can be achieved one-fourth of the dominant wavelength (Sheriff, 1977). Assume in this research, the GPR with 200MHz frequency can reach the best vertical (one-fourth of the wavelength), the vertical resolution of the data is about 0.2m.

For the horizontal resolution, the Fresnel zone plays an important role. Fresnel is an assumption of the covered zone of signal impulses with spherical wavefront. Usually, the horizontal resolution is defined as the width of the first Fresnel zone.

For calculating the Fresnel zone diameter, the propagation depth is essential since the wave energy is damping while traveling through the medium; thus, the horizontal resolution decreases with the increase of the depth. The width of Fresnel zone of GPR depends on the bandwidth, which is directly related to the center frequency f , the assumption of the horizontal resolution can be described as follows (Pearce and Mittleman, 2002):

$$A = \sqrt{\frac{D \cdot \lambda}{2}}$$

Figure 3.3 describes the theoretical model of the Fresnel zone.

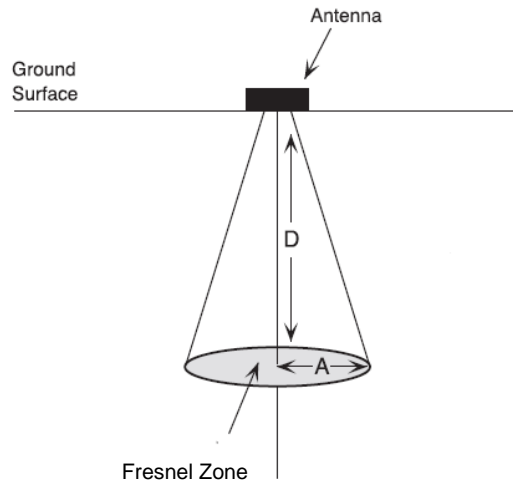


Figure 26. The theoretical model of the Fresnel zone

From the research of H.Hausmann and M. Behm (2011), the Fresnel zone of a GPR system with 200MHz frequency, the diameter is 2.9m with a depth of 5m. In this research, the depth record is up to about 19 meters; thus the horizontal resolution up to 5 meters is insufficient. From the theoretical model, the data resolution in this research is up to 6.1m.

As the accuracy of GPR data can also be influenced by the distortions and displacements of the impulse, we assume the data migration can efficiently compensate these defecations on data accuracy.

3.3 Feature Points Extraction

In this research, the depth interpolation can only proceed if isolated feature points of depth are selected from continuous depth profiles. The selection method is semi-automatic picking, combining auto-select and manual picking, since automatic selection algorithm with a threshold is not applicable for all the profiles, due to the complexity and the vast depth difference on individual profiles. The definition of feature points includes two ideas: isometric/equidistance selected points and points of interested.

The isometric selection criteria is a combination of two automatic selection methods, which are the isometric selection and equidistance selection. The isometric method picks a depth point at a length of every 10 percent of the distance of a profile from the start. Comparing using equidistance selection solely to the usage of isometric selection, it prevents both data redundancy and insufficient sampling. For the survey lines obtained in this research, so to say the profiles, vary enormously on lengths, from less than 1 meter to over 50 meters. If the sampling distance is set to less than 1 meter, there will be numerous profiles with single sampling point while some profiles have an unnecessary sampling density. For ensuring every profile has a sufficient sampling density, the isometric selection is necessary.

For the long profiles (longer than 20 meters), the sampling distance is longer than 2 meters, which is apparently too long, considering the horizontal resolution of the data. From H. Hausmann and M. Behm (2011), the 200MHz GPR has a 2.9m resolution at a depth of 5 meters, in this research, there is a considerable number of depth records which are more in-depth than 5 meters. Thus, with a sampling distance longer than 2 meters with a solely isometric selection, the Fresnel zones of the individual sample points will not have overlaps in the direction of the profile. Therefore, the densification of isometric selected points is necessary; the resampling method is chosen as an equidistance sampling with a 2 meters sampling distance on the profiles longer than 20 meters.

Once the depth points are chosen on the map, the corresponding points will be chosen on the data processing software, then input the depth of chosen points into the geo-information system.

For the manual picking, constructing a clear layer of the subsurface is necessary at first. The subsurface layers were also drawn manually since the migrated profiles provide satisfactory accuracy on spatial features, moreover, the gain function gives the data a sufficient contrast

for differencing the ice body and the subsurface. An example of manual picking on the data processing software is showed in *Figure 27*.

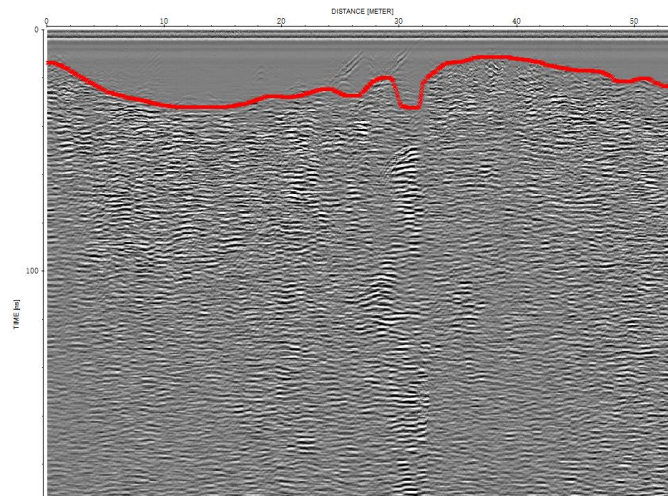


Figure 27. Example of subsurface manual picking

After the ice basement layer is chosen, a simplified layer can be constructed with velocity information as showed in *Figure 22*. The selection of points of interest can proceed from the layer. From the GPR profiles, the ice basement has an enormous complexity on the terrain surface, for the selection of points of interest under the complexity, there are four focuses:

- Discontinuity
- Distinguishable hollow structure
- Maximum depth point

For example, in the dataset of *Figure 28*, the points of interest are chosen by the three criteria mentioned.

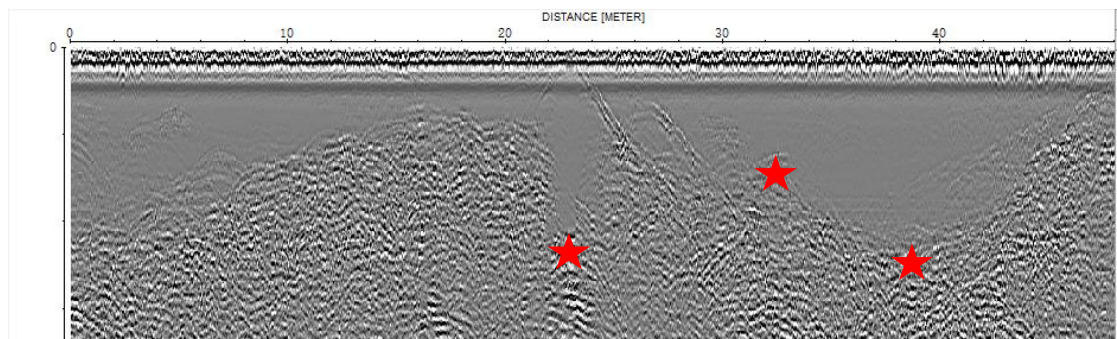


Figure 28. Example of feature points picking

As marked with red stars, the additional chosen points of interest from left to right, the first point is picked as the bottom of a clear hollow structure. Obviously, the hollow structure discontinues the adjacent surface. The second point is chosen according to its discontinuity with adjacent features as well. The last is the possible deepest point of this profile.

With the criteria of feature point selection, overall 1140 points were selected. The average depth of the selected points is 2.97m, with the average depth, the diameter of Fresnel zone is wider than 2 meters, the sampling distance, and thus the existence of overlaps between feature points on the direction of profiles can be insured.

3.4 Methodology of Depth Interpolation

For data interpolation, there are two broad classes of interpolation methods: deterministic and probabilistic (K. Krivoruchko, 2012). The deterministic methods interpolate a certain area with the pre-defined equation on the distance between the recorded data points and its adjacent area, the most known example of deterministic interpolation method is inverse distance interpolation (IDW). Different from the deterministic methods, probabilistic methods are based on spatial statistical theories. The statistic model predicts the quantities of the interpolated values with calculated possibilities. For the interpolation of ice thickness, so to say the ice basement surface, it is hard to define a direct relationship between the observed depth and the adjacent area due to the terrain complexity. Thus, the probabilistic interpolation methods are the ideal models for ice basement interpolation.

The Empirical Bayesian Kriging is chosen as the interpolation method in this study. EBK is modified from classic Kriging, which is a class of statistical techniques for optimal spatial prediction developed by Lev Gardin in 1959. Kriging predicts the spatial correlations between the value prediction and the distance by a function called semivariogram, which calculates the half of the average squared difference of the values of all the pairs of measurements at locations separated by a given distance. With the average values of these predictions, a matching semivariogram model can be constructed to predict the new values at unsampled locations.

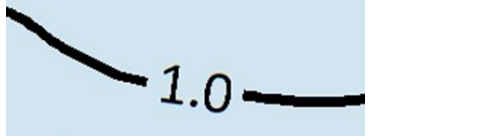


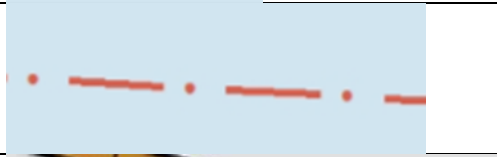

The Empirical Bayesian Kriging differs from classic Kriging by accounting for the error introduced by estimating the semivariogram model. Rather than using only one semivariogram

model, the EBK uses many of them for reaching a better prediction. Especially with a relatively big scale map with complex feature details, the estimation based on multiple semivariograms is more reliable on accuracy.

3.5 Methodology of Map producing

For the thematic maps focus on illustrating the ice thickness, also estimated details of ice basement, a classic contouring methodology is used. There are three levels of contours with different weight: first, the major contours with 2-meter intervals, which gives a brief overlook on the distribution of the ice thickness; second, contours with 1-meter intervals are the main strength to display the ice thickness with a satisfactory density and accuracy; last, the 0.5-meter interval contours were drawn to assist the demonstration of the whole map to reach a better accuracy by giving a more compact density of contours.

The overlook map of ice covered part of ERW cave used the rectified laser-scanned image as the base map to show the high geomorphic complexity of the cave not only the ice surface, also the tunnel wall and the rock breaking down on the ground, which are hard to represent in the thematic maps. The symbology system used in the final maps are showed in the table below:

Feature Class	Symbol
Depth contour with 2-meter interval	
Depth contour with 1-meter interval	
Depth contour with 1-meter interval	
GPR survey lines	
Walking path	

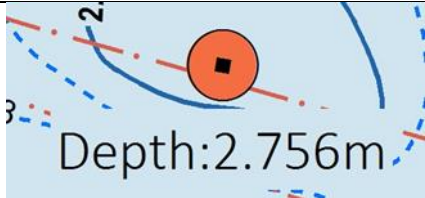
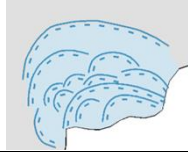

Point of interest (POI)	
Ice fall	
Breccia	

Table 3. Map symbols

4 RESULTS

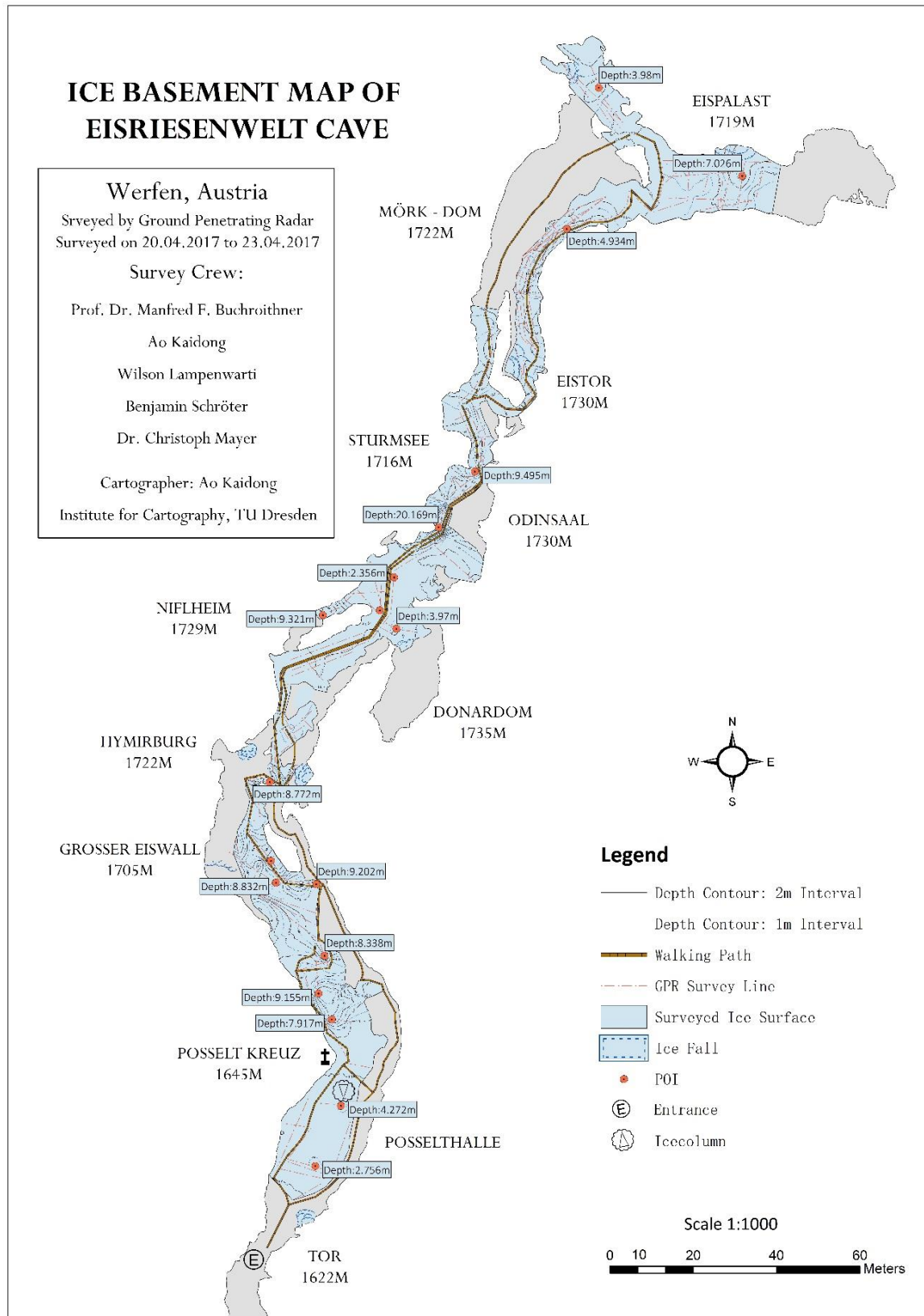


Figure 29, Ice basement map of Eisriesenwelt

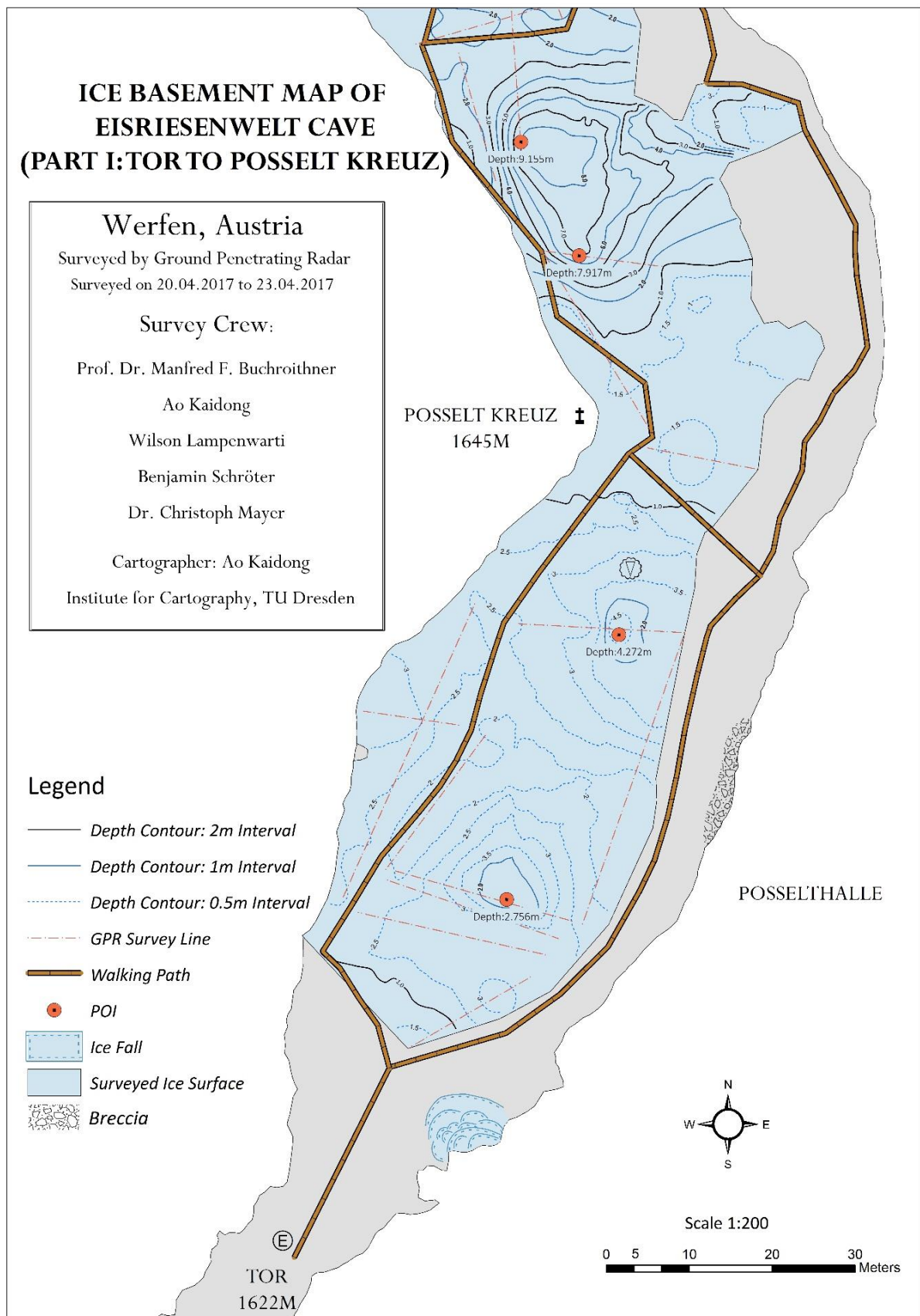


Figure 30. Thematic map of ice thickness (Part I)

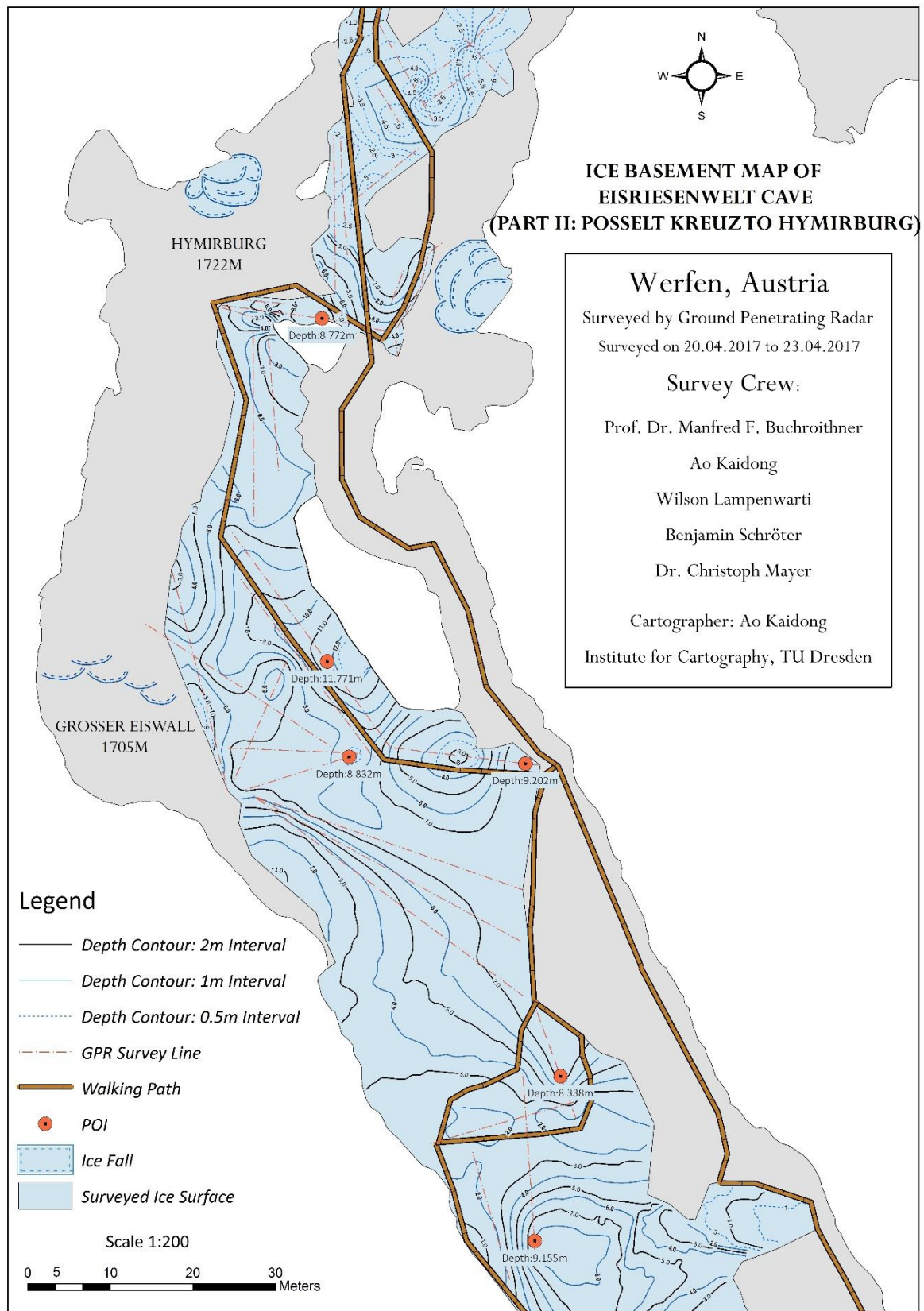


Figure 31. Thematic map of ice thickness (Part II)

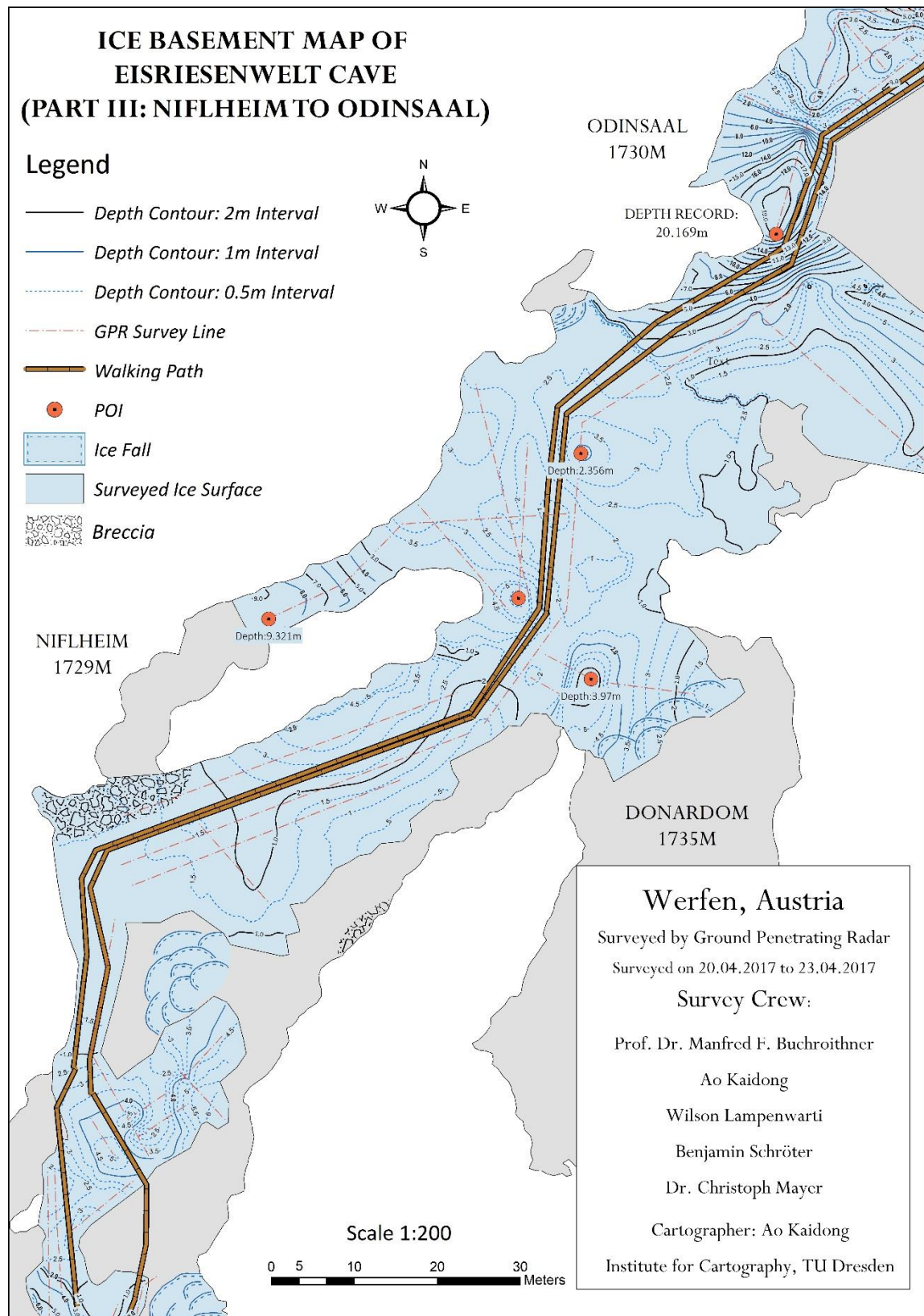


Figure 32. Thematic map of ice thickness (Part III)

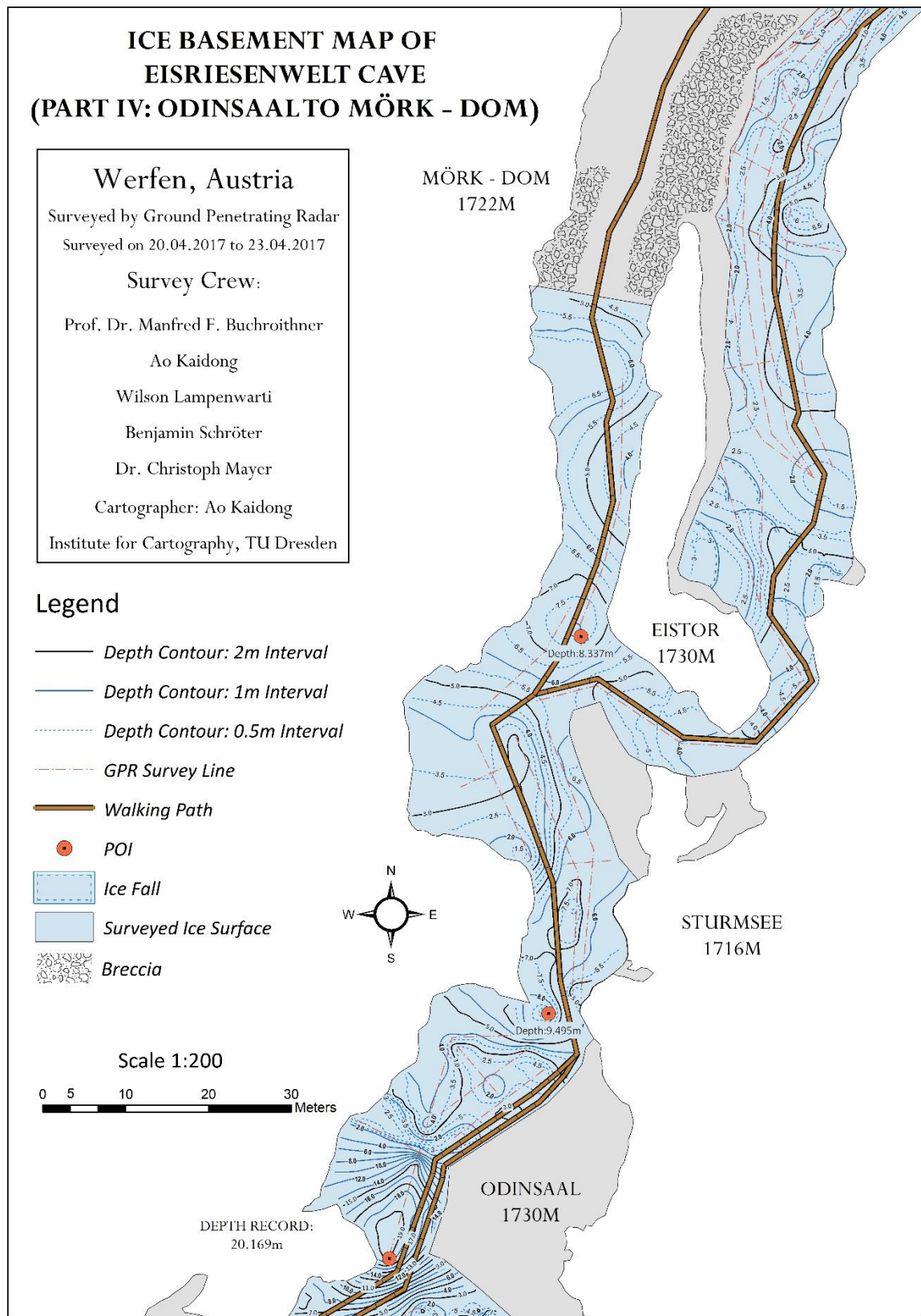


Figure 33. Thematic map of ice thickness (Part IV)

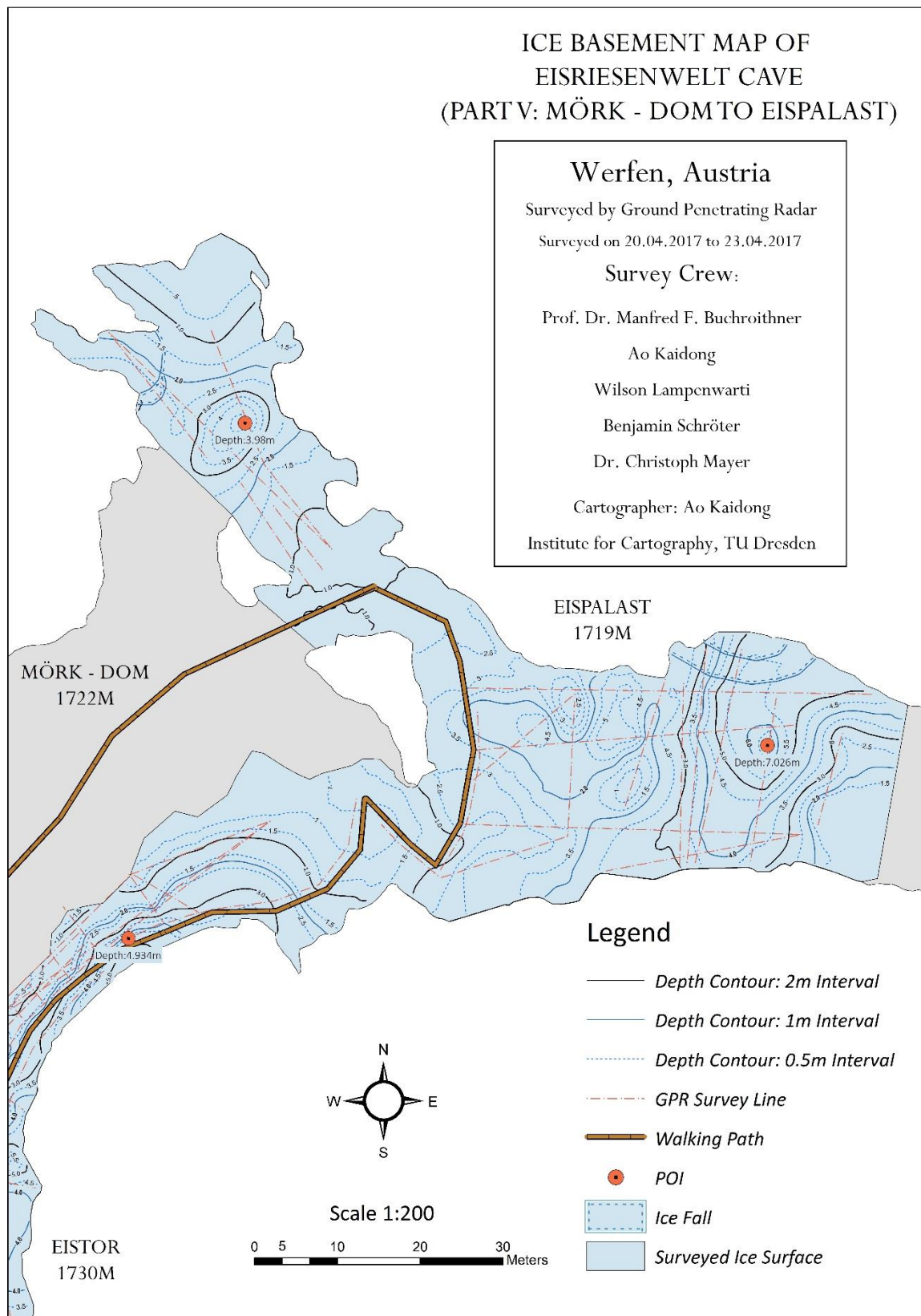


Figure 34. Thematic map of ice thickness (Part V)

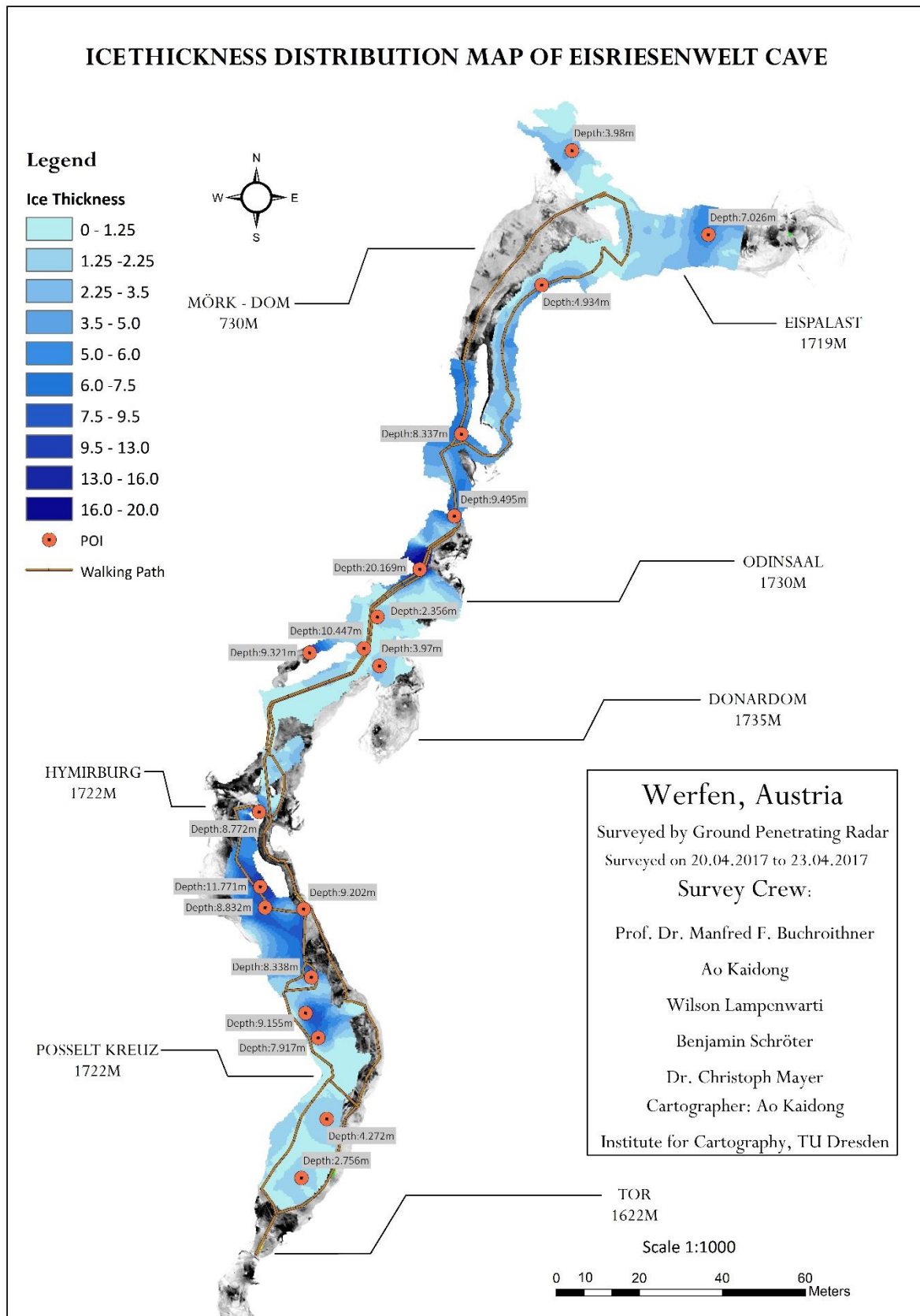


Figure 35. Ice thickness distribution map of Eisriesenwelt

5 CONCLUSION AND OUTLOOK

5.1 Conclusion

In this thesis, a procedure of the research on ice basement mapping is demonstrated, from data collecting to map producing. During the field trip, the planned survey lines covers a considerable percent of the ice coverage area, a solid base of the whole study was built. The raw data obtained during the field trip showed a satisfactory quality for pre-processing, even though the procedure of data pre-processing was standardized by former researchers, some flexible adjusts were still made in this research for exploiting the potentials of the raw data. With the given results on data migration, the specific migration method which was chosen in this thesis can be proven to be effective. With the semi-automatic sampling method which was created in this thesis, the depth information was extracted in point format. Calculation of the estimated depth obtained a reasonable result also because of the successfully extracted depth information.

As for the original aim of this study is to produce map series to illustrate the ice thickness with the GPR data, five thematic maps focus on the ice thickness, and an overlook map covers the whole ice-covered part of the ERW cave were made as the result of this thesis. For practical usage, the thematic maps can provide a detailed ice thickness distribution of the ERW cave, which can provide support on the future research focus on the ice volume. Furthermore, the contour maps can also be recognized as indicators to the subsurface form, which have a potential to provide evidence to future research focuses on geological topics of ERW. Also, the workflow of this research can provide a good example for future researchers of the similar topics.

The colour rendered map gives an overview of the ice thickness distribution, but not quantified. Which can serve the demonstrating works on ERW cave.

However, this study has its limitation. For example, due to some technical problem, most of the readings of the altitude meter in the laser scanning device were unavailable. Without a detailed elevation data on the ice surface, the overall profile of the ice-covered part of ERW cannot be produced. Moreover, it is found difficult to combine the 3D model with the GPR scanned data due to the difference of data format and geometric correcting. Due to the lack on surveying instruments, the survey lines were digitalized manually from the field note; which may cause a decreased accuracy on survey line positions and lengths.

5.2 Outlook

It is a pity that this thesis research did not reach the 3D modelling part due to the problems on multi-source data combining. With the data obtained in this research, the possibility of building a 3D ice thickness model is clear, which can be a potential research direction in the future.

References

- Annan, A. P. (2005). Ground-penetrating radar. In *Near-surface geophysics* (pp. 357-438). Society of Exploration Geophysicists.
- Annan, A. P. (2002). GPR—History, trends, and future developments. *Subsurface sensing technologies and applications*, 3(4), 253-270.
- Annan, A. P. (1999). Practical processing of GPR data. *Sensors and software, Ontario*.
- Arcone, S. A., & Delaney, A. J. (1989). *Investigations of dielectric properties of some frozen materials using cross-borehole Radiowave pulse transmissions* (No. CRREL-89-4). COLD REGIONS RESEARCH AND ENGINEERING LAB HANOVER NH.
- Behm, M., & Hausmann, H. (2008, May). Determination of ice thicknesses in alpine caves using georadar. In *Proceedings of the 3rd International Workshop on Ice Caves, edited by: Kadebskaya, O., Mavlyudov, BR, and Pyatunin, M., Kungur, Russia* (pp. 70-74).
- Berenguer-Sempere, F., Gómez-Lende, M., Serrano, E., & de Sanjosé-Blasco, J. J. (2014). Orthothermographies and 3D modeling as potential tools in ice caves studies: the Peña Castil Ice Cave (Picos de Europa, Northern Spain). *International Journal of Speleology*, 43(1), 35.
- Binder, D., Brückl, E., Roch, K. H., Behm, M., Schöner, W., & Hynek, B. (2009). Determination of total ice volume and ice-thickness distribution of two glaciers in the Hohe Tauern region, Eastern Alps, from GPR data. *Annals of Glaciology*, 50(51), 71-79.
- Buchroithner, M. F., Milius, J., & Petters, C. (2011, July). 3D surveying and visualization of the biggest ice cave on earth. In *Proceedings of 25th International Cartographic Conference* (Vol. 811).

- Christin Petters (2012). Eisriesenwelt: Processing steps from laser scanner point cloud to a photo-realistic three-dimensional model of the world's largest ice cave and presentation on an autostereoscopic 3D play. *Diploma Thesis of Institute of Cartography, TU Dresden*.
- Conyers, L. B., & Goodman, D. (1997). *Ground-penetrating radar* (pp. 149-194). An Introduction for Archaeologist: AltaMira Press.
- Eisen, O., Nixdorf, U., Wilhelms, F., & Miller, H. (2002). Electromagnetic wave speed in polar ice: validation of the common-midpoint technique with high-resolution dielectric-profiling and density measurements. *Annals of Glaciology*, 34(1), 150-156.
- Fisher, E., McMechan, G. A., & Annan, A. P. (1992). Acquisition and processing of wide-aperture ground-penetrating radar data. *Geophysics*, 57(3), 495-504.
- Galagedara, L. W., Redman, J. D., Parkin, G. W., Annan, A. P., & Endres, A. L. (2005). Numerical modeling of GPR to determine the direct ground wave sampling depth. *Vadose Zone Journal*, 4(4), 1096-1106.
- Geczy, J. and Kucharovic, L.: Determination of the ice filling thickness at the selected sites of the Dobsinska ice cave (in slovak, engl. summary). *Ochrana ladovych jaskyn Zilina*: 17–23, 1995.
- Hausmann, H., & Behm, M. (2010). Application of ground penetrating radar (GPR) in Alpine ice caves. *The Cryosphere Discussions*, 4(3), 1365-1389.
- Hubbard, B., & Glasser, N. F. (2005). *Field techniques in glaciology and glacial geomorphology*. John Wiley & Sons.
- Jol, H. M. (Ed.). (2008). *Ground penetrating radar theory and applications*. elsevier.
- Lehmann, F., & Green, A. G. (2000). Topographic migration of georadar data: Implications for acquisition and processing. *Geophysics*, 65(3), 836-848.

- Luetscher, M., Jeannin, P. Y., & Haeberli, W. (2005). Ice caves as an indicator of winter climate evolution: a case study from the Jura Mountains. *The Holocene*, 15(7), 982-993.
- Luetscher, M., & Jeannin, P. Y. (2004). Temperature distribution in karst systems: the role of air and water fluxes. *Terra Nova*, 16(6), 344-350.
- May, B., Spötl, C., Wagenbach, D., Dublyansky, Y., & Liebl, J. (2011). First investigations of an ice core from Eisriesenwelt cave (Austria). *The Cryosphere*, 5(1), 81-93.
- Neal, A. (2004). Ground-penetrating radar and its use in sedimentology: principles, problems and progress. *Earth-science reviews*, 66(3), 261-330.
- Obleitner, F., & Spötl, C. (2011). The mass and energy balance of ice within the Eisriesenwelt cave, Austria. *The Cryosphere*, 5(1), 245-257.
- Olhoeft, G. R. (2000). Maximizing the information return from ground penetrating radar. *Journal of Applied Geophysics*, 43(2), 175-187.
- Pearce, J., & Mittleman, D. (2002). Defining the Fresnel zone for broadband radiation. *Physical Review E*, 66(5), 056602.
- Podsuhin, N. and Stepanov, Y.: Measuring of the thickness of perennial ice in Kungur Ice Cave by georadar, in: Proceedings of the 3rd International Workshop on Ice Caves, edited by: Kadebskaya, O., Mavlyudov, B. R., Pyatunin, M., Kungur, Russia, 52–55, 2008
- Wu, T., Li, S., Cheng, G., & Nan, Z. (2005). Using ground-penetrating radar to detect permafrost degradation in the northern limit of permafrost on the Tibetan Plateau. *Cold Regions Science and Technology*, 41(3), 211-219.
- Yilmaz, Ö. (2001). *Seismic data analysis: Processing, inversion, and interpretation of seismic data*. Society of exploration geophysicists.